This is a preprint, the final version is subject to change, of the American Mineralogist (MSA)
Cite as Authors (Year) Title. American Mineralogist, in press.
(DOI will not work until issue is live.) DOI: http://dx.doi.org/10.2138/am-2014-4982

Revision 3

Combined geochemistry and geochronology constrains coupled subduction of oceanic and continental crust in the Huwan shear zone, central China

HAO CHENG [1,*] and JEFFREY D. VERVOORT [2]

[1]State Key Laboratory of Marine Geology, Tongji University, Shanghai 200092, China
[2]School of the Environment, Washington State University, Pullman, WA 99164, USA
[*] E-mail: oahgnec@gmail.com

ABSTRACT

Subduction of rocks into the mantle results in high-pressure metamorphism and the formation of eclogites from basaltic precursor rocks. In general, many kilometers of oceanic lithosphere are ultimately consumed prior to the subsequent continental slab subduction and collision. The exposure of the eclogites derived from oceanic subduction and continental subduction at the surface of Earth today record provide different P–T–t records of the subduction process. The Huwan shear zone in the Hong'an orogenic belt, marking a former ocean-continent transition zone, has been the focus of many studies on subduction-related high-pressure metamorphism. In this study, Lu–Hf garnet, U–Pb zircon, and Ar–Ar mica ages are combined with geochemical data to understand the origin of two coexisting eclogite bodies exposed along the Xuehe River in the Huwan Shear zone. In total, the results indicate that the two eclogites have different protoliths but experienced a similar metamorphic history. This observation requires new tectonic model for the coupled subduction of oceanic and continental crust in subduction zones. Combined geochemistry and zircon U–Pb geochronology suggest distinct oceanic and continental affinities for the eclogite protoliths. The Lu–Hf dates of 261.5 ± 2.4 Ma of the continental-type eclogite and 262.7 ± 1.7 Ma of the oceanic-type eclogite reflect garnet growth and are interpreted to closely approximate the age of eclogite-facies metamorphism. Therefore, both the geochemically oceanic- and continental-type eclogites underwent the same episode of Permian eclogite-facies metamorphism. The Permian Lu–Hf ages of *ca*. 262 Ma and the obtained Triassic Ar–Ar ages (~240 Ma) of the oceanic-type and continental-type eclogites imply coupled subduction and exhumation of oceanic and continental crustal materials in the Hong'an orogenic belt during the Permian and the Triassic. Though limited, the geochemical and geochronological results of this study, together with the discrepant Carboniferous dates for the nearby eclogites of previous studies, apparently suggest that the Huwan shear zone was not always a single coherent unit but rather comprises different tectonic slices that were metamorphosed at different times before final assembly. Some slices of the oceanic and continental crust underwent two subduction cycles during the Carboniferous and the Permian, whereas some eclogites registered only a single subduction-exhumation loop during the convergence between the South China Block and the North China Block in the Huwan shear zone. The consistent ages of the oceanic- and continental-type eclogites disfavor the traditional mélange model that high-pressure rocks are dismembered fragments that have been assembled and intercalated with rocks devoid of any high-pressure history at shallow crustal levels, forming a tectonic mélange.

Keywords: Lu–Hf, Huwan shear zone, eclogite, geochronology.

INTRODUCTION

Subduction of oceanic and continental crust eventually leads to the closure of back-arc basins and arc-continent and continent-continent collisions (O'Brien 2001; Ernst 2005), forming various types of high-pressure and ultrahigh-pressure (UHP) metamorphic rocks. Constraining the timing of the transition from subduction of oceanic to continental lithosphere is essential to understanding the details of this polyphase evolution. This can be done by dating the metamorphic rocks with both oceanic and continental affinities in the same collision zone.

The collision between the South China Block and the North China Block formed one of the largest UHP metamorphic belts in the world (Fig. 1a). The initiation of continental subduction has been traced back to late Permian ages of *ca*. 256 Ma (cf., Liu et al. 2008; Cheng et al. 2011) by dating the UHP/HP eclogites with continental affinity with a variety of geochronological methods, such as Sm–Nd, Lu–Hf, Ar–Ar and U–Pb. However, the time of the oceanic subduction prior to the onset of continental subduction remains controversial because geochronology of the oceanic-type metamorphic rocks within this belt yielded Carboniferous U–Pb zircon ages (Wu et al. 2009; Liu et al. 2010; Cheng et al. 2009) as well as Permian Lu–Hf and Sm–Nd ages (Cheng et al. 2009, 2013; Brouwer et al. 2011). Should the age discrepancies among high-pressure rocks of oceanic affinity suggest two distinct high-pressure metamorphism episodes or indicate a prolonged/episodic high-pressure metamorphism lasting from Carboniferous towards Permian? The Carboniferous U–Pb zircon ages for a continental-type eclogite appear to require final closure of the oceanic basin prior to *ca*. 310 Ma (Liu et al. 2010). Therefore, further studies on HP metamorphic rocks, especially the Carboniferous eclogite with a continental affinity, are required to clarify the geochronological enigma of this UHP terrane.

Lutetium-Hf garnet geochronology has become increasingly valuable as a routine tool to date metamorphic events with the improvement of the technology over the past few decades (Duchêne et al. 1997; Lapen et al. 2003; Skora et al. 2006; Kohn 2009; Mulcahy et al. 2009; Herwartz et al. 2011; Zirakparvar et al. 2011; Smit et al. 2013; Baxter and Scherer 2014). Garnet is well suited for combined chronological and thermobarometric research because of its ability to preserve original chemical and isotopic compositions in relatively low- and medium-temperature metamorphic rocks (e.g., Spear and Selverstone 1983; Ague and Carlson 2013; Massonne 2013; Baxter and Caddick 2013). Garnet is ideal for Lu–Hf geochronology because this phase strongly partitions Lu over Hf (Otamendi et al. 2002) and also because of its (presumed) high closure temperature (Dodson 1973; no less than 900 °C, Skora et al. 2009, Smit et al. 2013; Shu et al. 2013). The high affinity of garnet for Lu may produce strong core-to-rim zonation in Lu, resulting in Lu–Hf ages that are biased toward the early (prograde) garnet growth (Lapen et al. 2003). Any age determined by Lu–Hf garnet geochronology depends on how accurately the analyzed garnet separates reflect the complete garnet chemistry within the rock. To specify the geological meanings of these ages, bulk rock/inclusions bearing inherited Hf, complexities in garnet growth and post-garnet crystallization resetting must be clarified carefully (Cheng et al. 2012). REE zonations in garnet, coupled to crystal size distributions, provide a powerful means for understanding prograde metamorphic paths when combined with Lu–Hf geochronology (Skora et al. 2008).

In this study, we investigated two newly identified eclogites collected along the Xuehe River (west of the Huwan shear zone, Hong'an orogenic belt; Fig. 1b). These rocks are of both oceanic and continental affinity and were selected for combined garnet Lu–Hf, zircon U–Pb and phengite Ar–Ar geochronology. The preservation of the growth zoning indicates that the garnet Lu–Hf ages directly date the prograde metamorphism and garnet growth. Here we document Permian Lu–Hf dates and Triassic Ar–Ar ages of the oceanic-type and continental-type eclogites, suggesting coupled subduction and exhumation of oceanic and continental crustal materials in the Huwan shear one during the Permian and the Triassic, respectively. Our results suggest that under specific circumstances, high-pressure rocks of diverse protoliths from a single orogenic belt, may undergo similar multiple subduction-exhumation cycles.

GEOLOGICAL SETTING

The Paleozoic convergence between the South China Block (SCB) and the North China Block (NCB) is associated with a series of tectonic processes such as oceanic subduction, terrane accretion and continental collision, and resulted in the Qinling–Tongbai–Hong'an–Dabie–Sulu orogenic belt (Fig. 1; Zhou et al. 1993; Webb et al. 1999; Meng and Zhang 1999; Sun et al. 2002; Zheng et al. 2006, 2012; Ratschbacher et al. 2006; Wu et al. 2009, 2013). The Dabie–Sulu orogenic belt is characterized by the occurrence of Triassic UHP eclogite-facies metamorphic rocks due to the Triassic continental deep subduction in east-central China. However, no juvenile arc terrane has been found between the SCB and the NCB in this belt so far, indicating this continental subduction zone was largely a Triassic continent–continent collisional orogen. On the other hand, there are Paleozoic tectonic events of arc–continent collision in the Qinling–Tongbai–Hong'an orogenic belt in central China that were followed by the late Permian to early Triassic continental collision (e.g., Mattauer et al. 1985; Kröner et al. 1993; Ratschbacher et al. 2006; Cheng et al. 2012). As a consequence, the Qinling–Tongbai–Hong'an orogenic belt in the west exhibits a series of tectonic differences from those in the Dabie–Sulu orogenic belt in the east (Meng and Zhang 1999; Ratschbacher et al. 2006; Wu et al. 2013). The Hong'an orogenic belt was previously named as Western Dabie in the literature, but we prefer to call it as the Hong'an orogenic belt because of significant differences in protolith nature and metamorphic style from the Dabie orogen, which resulted from the collision between the North China Blocks and the South China Block (Fig. 1a). High-pressure and UHP eclogites are found throughout the Hong'an orogenic belt (e.g., Zhou et al. 1993; Hacker et al. 1998). Metamorphic grade and peak pressures generally increase northward from transitional blueschist–greenschist in the south, through epidote–amphibolite and quartz eclogite to coesite eclogite in the north, reflecting apparently down-to-the-north subduction (Ratschbacher et al. 2006).

The Huwan mélange (Ratschbacher et al. 2006) or Huwan shear zone (Sun et al. 2002) in the Hong'an orogenic belt, spanning ~65 km east to west and ~6 km north to south, marks the tectonic contact between the more inboard Qinling–Tongbai orogenic belt to the northwest and the outboard Dabie–Sulu orogenic belt in the southeast. The Sujiahe unit, in the north of the Huwan shear zone, consist of tectonic slices of ultramafic rocks, gabbros, basalts, and diabasic dikes, which likely represent a former ophiolite sequence now dismembered into various-scale fragments that are now in fault contact (Ye et al. 1993; Wu et al. 2013). The ophiolites have been interpreted to be of Carboniferous age based on foraminifera in interlayered marbles (Ye et al. 1994). The Huwan shear zone is thus considered to form in an oceanic marginal basin (Wu et al. 2013) and taken as a subduction-accretion complex containing elements of the Qinling microcontinent and its arc, the Paleotethyan ocean floor, and possibly the South China Block (Ratschbacher et al. 2006), although there are no detailed isotope compositions and formation ages for the mafic rocks.

Eclogites occur as massive outcrops with no obvious lithological contacts or occasionally as layers and lenses surrounded by metasediments in the Huwan shear zone (Liu et al. 2004; Xu et al. 2000; Gao et al. 2002; Sun et al. 2002). Peak eclogite-facies metamorphism has been constrained to 1.4–2.1 GPa and 540 °C to 730 °C, followed by a retrograde greenschist- to amphibolite-facies overprint (Fu et al. 2002; Liu et al. 2004; Ratschbacher et al. 2006; Cheng et al. 2009, 2010, 2013; Brouwer et al. 2011). The eclogite and the surrounding metasediments have been subjected to the same retrograde metamorphic processes (Xu et al. 2000), but no clear relationship between them has been directly observed in the field. Zircons from the granitic gneiss yield a protolith formation age of 738 ± 6 Ma (Liu et al. 2010), which is typical Neoproterozoic basement rock of the South China Block (Hacker et al. 1998).

Eclogites in the Huwan shear zone have both typically mid-ocean ridge and island arc basalt-like trace element patterns and with generally positive whole-rock $\varepsilon_{Nd(0)}$ values up to +7.4 and corresponding high $\delta^{18}O$ values of +8.8 to +11.2 ‰ (Li et al. 2001; Fu et al. 2002; Gao et al. 2002; Cheng et al. 2009, 2013; Wu et al. 2009). The geochronological data collected from the Huwan eclogites provide an apparently conflicting picture of the timing of the eclogite-facies metamorphism. This most likely indicates that the Huwan shear zone was involved in a complex process of collision and exhumation during the convergence between the North China Block and the South China Block. It has been suggested that the zircon U–Pb ages for the eclogites with oceanic affinity record high pressure metamorphic events that spread over 200 Myr from Silurian to Triassic (Jian et al. 1997, 2000; Sun et al. 2002; Liu et al. 2004; Cheng et al. 2009; Wu et al. 2009; Liu et al. 2011). A Carboniferous U–Pb age of *ca*. 310 Ma has also been determined for a metamorphic zircon of an eclogite of continental affinity (Liu et al. 2011). Garnet Lu–Hf and Sm–Nd dates of oceanic eclogites range from 270 Ma to 252 Ma (Cheng et al. 2009, 2010, 2013; Brouwer et al. 2011). A much older garnet whole rock Sm–Nd isochron with an age of 422 ± 67 Ma for the Huwan eclogite (Ye et al. 1993) shows evidence for a significant contribution from the REE-rich phases in the garnet fractions that result in lower $^{147}Sm/^{144}Nd$ ratios (<0.3). The older garnet whole rock Sm–Nd ages in comparison to later Sm–Nd results (Cheng et al. 2009, 2010, 2013; Brouwer et al. 2011) imply that the inclusions were not in equilibrium with the garnet and the older Sm–Nd age is likely geologically meaningless. The timing of cooling and deformation of the Hong'an HP rocks has been constrained by Ar–Ar analyses of synkinematic minerals from the Huwan shear zone at *ca*. 206 Ma (Webb et al. 1999) and *ca*. 235–195 Ma (Ratschbacher et al. 2006), respectively.

SAMPLES ANALYZED

The two eclogite samples examined in this study were collected along the Xuehe River (Fig. 1b-f; 31º47′ N, 114º35′ E). The eclogites exist as lens-like bodies (~3 meters across) in the granitic gneiss (Fig. 1d-f). The two eclogites are fresh and composed mainly of a similar mineral assemblage of garnet, omphacite, quartz and phengite, with minor amphibole, epidote and rutile. One eclogite (c79) is a coarse-grained and green-colored eclogite. A second eclogite (c81) was sampled ~300 m north from the sample c81 along the river and is fine-grained and dark-colored, and has a similar mineralogy assemblage but much smaller garnets and more omphacites in comparison to sample c79. The garnet–omphacite–phengite–quartz assemblage is representative of the peak metamorphic conditions of the Xuehe eclogites. These rocks were selected for combined garnet Lu–Hf, zircon U–Pb and phengite Ar–Ar geochronology.

ANALYTICAL STRATEGY

Major and trace element compositions of whole rocks were analyzed at the Washington State University to classifying their protoliths. Major elements were determined by spectrometry using a ThermoARL X-ray fluorescence spectrometer (XRF). Trace elements were determined using an Agilent 4500 quadrupole inductively coupled plasma mass spectrometer (ICP-MS). Analytical errors (RSD%) for the major elements were 1–2% (1σ) or smaller. These were generally less than 3% for high field strength elements and 5% for other trace elements.

To linking garnet Lu–Hf age and zircon U–Pb age with specific metamorphic episodes, electron microprobe was applied to characterize the major elemental distribution in garnets and LA-ICP-MS was used to characterize the distribution of select trace elements in garnets and zircons. Major element compositions of garnets and other minerals were obtained using a JEOL JXA-8100 electron microprobe operating at 15 kV, at the China University of Geosciences. Natural and synthetic standards (SPI^{TM}) were used to calibrate all quantitative analyses and a ZAF correction was used for data reduction. The distribution of select trace elements in garnet porphyroblasts and zircons were determined using laser-ablation ICP-MS at the State Key Laboratory of Geological Processes and Mineral Resources at the China University of Geosciences. Garnets and zircons were analyzed using a pulsed 193 nm ArF Excimer laser with 14 J·cm^{-2} energy density at a repetition rate of 8 Hz coupled to an Agilent 7500 quadrupole ICP-MS with a spot size of 32 μm. External calibration was performed relative to multiple-reference materials (BCR-2G and BHVO-2G for garnet; GJ-1 and NIST 610 for zircon) combined with internal standardization (Si for garnet and Zr for zircon; Hu et al. 2011). Off-line selection and integration of background and analytic signals and time-drift correction and quantitative calibration were performed using *ICPMSDataCal* (Liu et al. 2008b). The USGS SRM BIR-1G glass standard was used to monitor external reproducibility and instrument drift. During the time-resolved analysis of minerals, anomalies resulting from inclusions, fractures, and zones of different composition were monitored using several elements, and only the relevant part of the signal was integrated. Analyses of rock standards (BCR-2G, BHVO-2G, GJ-1, NIST 610) indicate that the precision (RSD%) is better than 10% (2σ) for the rare earth elements.

For zircon U–Pb isotope analyses, zircon 91500 (Wiedenbeck et al. 2004) was used as external standard for U–Pb dating and was analyzed twice every 5 analyses. Time-dependent drifts of U–Pb isotopic ratios were corrected using a linear interpolation (with time) for every fifth sample analysis according to the variations of the four 91500 analyses (Liu et al. 2011). The uncertainty of the preferred value for the external standard 91500, which was 0.9–1.3% (1σ RSD) for $^{206}Pb/^{238}U$, was propagated to the ultimate results of the samples.

Ar–Ar chronometer is used to unravel the cooling history the Xuehe eclogites. The argon isotope ratios of phengite were analyzed using a GVI-5400® noble gas mass spectrometer in the Guangzhou Institute of Geochemistry, Chinese Academy of Sciences, using the stepwise crushing technique (Qiu and Wijbrans 2006). Samples and monitor standard DRA1 sanidine (Wijbrans et al. 1995) with an assumed age of 25.26 ± 0.07 Ma were irradiated at the 49–2 reactor in Beijing for 54 h. The crusher consists of a 210 mm long, 28 mm bore diameter high-temperature resistant stainless steel tube (T_{max} ~1200 ^{o}C). The extraction and purification lines were baked out for about 10 h at 150 ^{o}C with heating tape and the crusher at 250 ^{o}C with an external tube furnace. Experimental details can be found in Qiu and Wijbrans (2006).

For Lu–Hf geochronology, multiple garnet and whole-rock fractions, each consisting of ~250 mg of material, from each sample were dissolved in the radiogenic isotope clean laboratory at Washington State University. All garnet fractions and a whole rock powders from each sample were dissolved on a hotplate at ~110 °C in a concentrated HF and HNO_3 (10:1 ratio) acid mixture for either 2–3 days (garnet fractions) or 5–7 days (whole rock). A second whole rock powder for each sample was dissolved in a high-pressure, steel-jacketed Teflon capsule at 160 °C for 5–7 days in concentrated HF and HNO_3 (10:1). Following dissolution, samples were dried and converted from fluorides to chlorides using a mixture of H_3BO_3 and 6 M HCl. Each sample was then dried again and redissolved in only 6 M HCl. Small aliquots (5–10%) were taken from these solutions to test for elemental concentrations for ideal spiking and ^{176}Lu–^{180}Hf and ^{149}Sm–^{150}Nd tracers were added to these solutions and equilibrated. Subsequently Hf, Lu, Nd, and Sm were then isolated using established ion-chromatographic techniques (Vervoort et al. 2004). Aliquots of garnet fractions that had extremely low (i.e., ~ chondritic) Sm/Nd ratios were deemed unusable for Sm/Nd garnet geochronology and therefore not pursued further. Full discussions of the methods of dissolution, spiking, chemical separation, and analysis used in this study are in Cheng et al. (2008). The chemically separated Nd, Sm, Lu and Hf from each sample was dissolved in 2% HNO_3 and analyzed on a ThermoElectron Neptune™ multi-collector (MC–) ICP-MS in the GeoAnalytical Laboratory at Washington State University. The overall external uncertainties of 0.5% were applied to the measured $^{147}Sm/^{144}Nd$ and $^{176}Lu/^{177}Hf$ ratios based on the long-term reproducibility of the external rock standards. External uncertainties applied to the measured Nd and Hf isotope data are a combination of 2σ in-run error and a blanket 0.005% uncertainty added in quadrature for $^{143}Nd/^{144}Nd$ and $^{176}Hf/^{177}Hf$. The analytical precisions of the isotope ratio measurements are given as ±2σ. For the calculation of the depleted mantle model ages ($[T_{Nd}]_{DM}$), we use a ^{147}Sm decay constant of 6.54×10^{-12} a^{-1} (Lugmair and Marti 1978) and depleted mantle values $^{147}Sm/^{144}Nd$=0.2137 and $^{143}Nd/^{144}Nd$=0.51315 from Chen and Jahn (1998). For the calculation of the ε_{Nd} values, we use CHUR values of $^{147}Sm/^{144}Nd$=0.1960 and $^{143}Nd/^{144}Nd$=0.512630 from Bouvier et al. (2008). All Lu–Hf isochron ages were calculated using *Isoplot v4.15* (Ludwig 2008) and a ^{176}Lu decay constant of 1.867×10^{-11} a^{-1} (Scherer et al. 2001; Söderlund et al. 2004). Errors are reported at 95% confidence.

RESULTS

Bulk chemical composition

The major and trace element compositions of the two eclogites are provided in Table 1. The eclogites are characterized by low LOI contents, 0.63 wt.% and 0.68 wt.%, respectively. Both eclogites have similar basaltic major element compositions (SiO_2 = 46.3–48.1 wt.%; K_2O+Na_2O = 1.5–2.2 wt.%; Lebas 1989). Sample c81 has much higher compatible element concentrations than sample c79 (e.g., Cr = 423 ppm *vs.* 17.3 ppm).

Sample c81 has a REE pattern that is typical of normal mid-oceanic ridge basalts (N-MORBs) with slight light rare earth elements (LREEs) depletion and a flat heavy rare earth elements (HREEs) pattern, with a $(La/Nb)_N$ ratio of 1.1, approximately ten times chondritic abundances (Fig. 2a). The LREEs of sample c79 are slightly enriched with $(La/Yb)_N$=4.2, and the total REEs (ΣREEs) are considerably higher (150 ppm) than sample c81 (21 ppm). Sample c79 shows LREEs-enriched pattern, prominently enrichment of LILE, and distinct negative Nb-Ta and Zr-Hf anomalies and positive Pb anomalies (Fig. 2b), features typical of continental arc andesite.

The Nb-Ta and Zr-Hf contents of sample c79 are typical of upper continental crust (UCC) (Rudnick and Gao 2003) and contain fewer anomalies than sample c81. Sample c79 and c81 have a negative Ti peak and a contrasting positive Ti peak, respectively.

Sample c79 has a $^{143}Nd/^{144}Nd$ ratio = 0.512135 and $^{147}Sm/^{144}Nd$ =0.1495, corresponding to an $\varepsilon_{Nd(0)}$ value of -9.7 and an ancient $[T_{Nd}]_{DM}$ model age of 2.4 Ga (Fig. 2c and d). In contrast, sample c81 has a significantly more primitive Nd isotopic composition, with $^{143}Nd/^{144}Nd$ = 0.513015 and $^{147}Sm/^{144}Nd$ = 0.2315, which yields an $\varepsilon_{Nd(0)}$ value of +7.5.

Mineral compositions and *P–T* estimates

Garnets are porphyroblasts, with mostly idioblastic shapes, approximately 0.2–1.0 mm in size, and have quartz, epidote, and omphacite inclusions (Fig. 3). End-member components (mol%) were calculated on the basis of four components; pyrope (Pyr), almandine (Alm), spessartine (Sps) and grossular (Grs). Pyr = 100×Mg/(Mg + Fe^{2+} + Mn + Ca); Alm = 100×Fe^{2+}/(Mg + Fe^{2+} + Mn + Ca); Sps = 100×Mn/(Mg + Fe^{2+} + Mn + Ca) and Grs = 100×Ca/(Mg + Fe^{2+} + Mn + Ca). Garnets of both samples have high almandine contents (c79=$Alm_{50–64}Grs_{19–32}Pyr_{3–18}Sps_{0.5–17}$; c81=$Alm_{54–64}Grs_{26–36}Pyr_{3–10}Sps_{0.4–9}$; Fig. 3). Most euhedral, porphyroblastic garnets have pronounced compositional zoning with the garnet cores having much lower almandine and higher grossular contents. The compositional profiles of porphyroblastic garnets appeared to be continuous in both eclogites, showing typical prograde zoning with a gradual increase in pyrope and a decrease in spessartine from core to rim. Omphacite occurs as randomly oriented blocky crystals in textural equilibrium with the garnet. The jadeite (Jd) component of most omphacite ranges from 28 to 42 mol% in sample c79 and 31–37 mol% in sample c81 (Jd = 100×(Na – Fe^{3+})/(Ca + Na); Table 2), and individual fresh grain does not show noticeable chemical zonation. The Si concentrations of phengite range from 3.43 to 3.52 apfu for sample c79 and 3.45 to 3.55 apfu for sample c81 when normalized to 11 oxygen atoms. Minor retrograde textures involving the breakdown of omphacite to Ca–Na amphibole-rich symplectite were present. Lutetium is concentrated in the core and decreases toward the rim in selected garnet porphyroblasts from sample c79 and c81 (Table 3, Fig. 3d and 3h).

The *P–T* conditions of the Xuehe eclogite were estimated using conventional methods based on local equilibrium. The garnet–omphacite–phengite–quartz/coesite assemblage is representative of the peak metamorphic conditions of the Xuehe eclogite. Analyses of garnet rims (using maximum Mg# (Mg# = $Mg^{2+}/(Mg^{2+} + Fe^{2+})$)) and Si-rich phengite were used to estimate the peak temperature for eclogite-facies metamorphism. The conventional methods, Fe^{2+}–Mg exchange garnet–clinopyroxene thermometry (Krogh-Ravna 2000) and garnet–clinopyroxene–phengite–SiO_2 barometric calibration (Krogh-Ravna and Terry 2004; $Fe^{3+}{}_{cpx} = Na - Al_{total}$), were used for the P–T estimations. Garnet rim analyses with a maximum Mg apfu and the Si-richest phengite analysis were used to estimate the peak pressure and temperature for the eclogite-facies metamorphism. Where the rim compositions of garnet–omphacite pairs were found in textural equilibrium, the estimated maximum pressure and temperature interval were within the range of 2.0–2.2 GPa and 525–576 °C for sample c79 and 2.1–2.6 GPa and 506–554 °C for sample c81 within the quartz stability field (Fig. 4). The THERMOCALC3.33 average *P–T* calculation mode was applied for the assemblage of Grt+Omp+Phen (Table 2). The activities of mineral end-members were obtained using *AX*, as recommended by Holland and Powell (1998). Intersection mean values of 2.0 GPa and 532 °C (c79) and 2.3 GPa and 498 °C (c81) were defined in the simplified model system NCKFMASH with excess SiO_2 and H_2O; these values were largely consistent with the pressure–temperatures of the Grt+Omp+Phen assemblage using conventional methods and the previous calculations for other eclogites in the Huwan shear zone (e.g., Liu et al. 2004; Ratschbacher et al. 2006).

The garnet Lu–Hf isochrons, zircon U–Pb and element data and the corresponding Ar-Ar data for the two eclogites are presented in Figures 5–8, Table 4 and Supplementary Tables 5–7 (Appendix 1–3). The data regression and the uncertainties for the isotopic ratios were estimated as explained above in the analytical methods.

Lu–Hf results

The Lu–Hf age of the eclogites was based on the isochron defined by whole rock + garnet + omphacite. The Lu–Hf ages of the Xuehe eclogites are 261.5 ± 2.4 Ma for c79 (n = 6; four garnet fractions, one omphacite fraction, and one whole rock fraction; Mean Square Weighted Deviation (MSWD) = 0.8; Fig. 5a) and 262.7 ± 1.7 Ma for c81 (n = 7; six garnet fractions and one omphacite fraction; MSWD = 1.1; Fig. 5b). A selective tabletop-digestion procedure was applied to minimize dissolving zircon contained in the garnet and whole rock. Regression through the garnet, omphacite, tabletop-digested whole rock and bomb-digested whole rock separates for sample c79 yields a much lower initial $^{176}Hf/^{177}Hf$ value (Fig. 5a). The bomb-digested whole rock would bias the isochron to give an age that is too old and, therefore, is excluded from this regression. Inclusion of the whole rocks reduces the precision of the regression for sample c81 (265.0 ± 2.8 Ma; MSWD = 3.3) and yields a slightly lower initial isotopic value of 0.28310 ± 3 (Fig. 5b).

Zircon isotope and element data

Few zircon grains were extracted from sample c79. The zircon crystals in the Xuehe eclogite were subhedral, transparent, and colorless, with few inclusions and displaying rounded external habits with aspect ratios typically 1:1 and not exceeding ~1:2. The CL images for sample c81 clearly display CL-bright core domains and secondary alteration or an overgrowth rim with bright CL (Fig. 6a). The CL images for sample c79 show complex textures with internal domains containing a mix of bright to dark CL grey scale that display sectoral zoning and unzoned rims with weak CL.

The zircon trace element concentrations are highly variable and show little systematic inter-element variations except for a positive correlation between Th and U concentrations (Fig. 7). Forty U–Pb isotope analyses on 33 zircon grains from sample c81 yielded largely discordant U–Pb ages. U–Pb isotopic results are reported in Tera-Wasserburg concordia plot (Fig. 6a) as well as histograms and relative probability functions of ^{207}Pb-corrected dates (Ludwig 2008). Despite the apparent preservation of simple core and secondary domain relationships, there are no clear correlations between the analysis location and the ^{206}Pb/^{238}U ages. Using the Unmix function of *Isoplot* (Ludwig 2008), we identify two main age peaks at 390 ± 4 Ma to 449 ± 5 Ma for the concordant analyses (Fig. 6a). All analyses have high U (98–1280 ppm) and Th (11–215 ppm) concentrations and high Th/U ratios (0.07–0.22; Appendix 1). No correlations between Th/U ratio, internal texture/structure or age were recognized. Only six largely concordant U–Pb analyses are reported for 5 grains from sample c79 due to few extracted zircon grains (Appendix 1). Apparent ^{206}Pb/^{238}U ages spread from 714 ± 10 Ma to 822 ± 11 Ma, coupled with higher U and Th content and Th/U ratios (Th = 324–1794 ppm; U = 555–1850 ppm; Th/U = 0.3–1.4), yielding an average age of 753 ± 37 Ma (MSWD = 15). The REE contents (Appendix 2) for the zircon core and rim domains from sample c81 have enriched HREE patterns (Lu_N/Gd_N = 42–108, av. 80; Fig. 6b); sample c79 zircons have relatively flat HREE patterns (Lu_N/Gd_N = 11–38, av. 19).

Ar isotopic data

The phengite multi-grain laser step-heating analyses of c81 display fairly flat pattern, indicating homogeneous Ar-isotopic composition released through the experiment. Age calculation over all increments yielded an age of 242.6 ± 0.9 Ma (Appendix 3, Fig. 8). The $^{36}Ar/^{40}Ar$ *vs.* $^{39}Ar/^{40}Ar$ isotope correlation plot yields a y-axis intercept of $^{40}Ar/^{36}Ar$ = 282 ± 29, comparable to the present day atmospheric composition of Ar. The Ar release pattern of phengite for the sample c79 is slightly scattered. Age calculation over the first six increments, excluding the very first step, is 239.5 ± 0.6 Ma (Appendix 3, Fig. 8). A poorly defined inverse isochron yields an age 240.1 ± 10.4 Ma with atmospheric initial ratio.

DISCUSSION

Eclogites of the Huwan shear zone

The Qinling–Tongbai–Hong'an–Dabie–Sulu orogenic belt was segmented by a number of faults or sedimentary basins (Fig. 1). Each terrane contains a series of metamorphic units that can be correlated with each other. There are three kinds of eclogite in the Huwan shear zone, which have quite different geochemical characteristics (Li et al. 2001; Fu et al. 2002; Gao et al. 2002; Liu et al. 2004; Jahn et al. 2005; Cheng et al. 2009; Wu et al. 2009; Liu et al. 2010): (1) The first kind of eclogite is characterized by the MORB-like patterns of trace element distribution, highly positive $\varepsilon_{Nd(0)}$ and $\varepsilon_{Hf(0)}$ values, and high $\delta^{18}O$ values (Fu et al. 2002; Gao et al. 2002; Wu et al. 2009; Liu et al. 2011). Their protolith ages were constrained at *ca*. 400–430 Ma by zircon U–Pb dating (Cheng et al. 2009; Wu et al. 2009; Liu et al. 2010). These features indicate that their protoliths might have been derived from the Paleotethyan oceanic crust (Li et al. 2001; Fu et al. 2002; Gao et al. 2002; Wu et al. 2009; Liu et al. 2011). (2) The second kind of eclogite exhibits the arc-like patterns of trace element distribution and positive $\varepsilon_{Nd(0)}$ values; their protolith were considered as Neoproterozoic island arc basalts (Li et al. 2001) or oceanic basalts that experienced different degrees of crustal contamination (Wu et al. 2009). (3) The third kind of eclogite exhibit enriched compositions of trace elements and radiogenic isotopes (Jahn et al. 2005) with protolith ages of 716 ± 28 to 766 ± 14 Ma (Hacker et al. 1998, 2000; Liu et al. 2004, 2011). Their protoliths were suggested to be the continental crust from the SCB (Zheng et al. 2006).

The coexistence of the Paleozoic oceanic crust and Neoproterozoic continental crust in the Huwan shear zone can be explained by splitting of the Neoproterozoic continental crust from the northern part of the SCB and production of the Paleozoic oceanic crust within an oceanic marginal basin close to the SCB (Wu et al. 2013).

Protolith of the Xuehe eclogite sample c79

Major element compositions of the studied eclogites and their mineral assemblages indicate that the protoliths for the Xuehe eclogites were most likely of basaltic composition. The two Xuehe eclogites show contrasting trace elemental and isotopic features.

Sample c79 shows elemental and isotope signatures, such as the LREE-enriched profiles, depleted high field strength elements relative to large ion lithosphere elements, and a negative $\varepsilon_{Nd(0)}$ value (Fig. 2); all these are consistent with a continental origin (Rudnick and Gao 2003). These features are common to those eclogites with continental affinity across the

Hong'an–Dabie–Sulu terranes (Jahn 1998). Sm–Nd isotopic data for sample c79 yield a Paleoproterozoic $[T_{Nd}]_{DM}$ model age of 2.4 Ga, which is consistent with Proterozoic $[T_{Nd}]_{DM}$ model ages between 1.8 and 2.5 Ga for metamorphic rocks across the South China Block (e.g., Chen and Jahn 1998; Bryant et al. 2004). The magmatic zircon in sample c79, yields an apparent protolith U–Pb age of 753 ± 37 Ma (Fig. 6a). These Neoproterozoic dates resemble the relict magmatic zircon cores ages from the HP/UHP metamorphic rocks across the Dabie-Sulu terrane (e.g., Zheng et al. 2006; Liu et al. 2011) and are similar to typical Neoproterozoic basement rocks of the South China Block (Hacker et al. 2000). We thus conclude that the protolith of this eclogite was formed within a continental setting, derived from reworking of the late Mesoproterozoic crust of the South China Block, and corresponded to bimodal magmatism in rifting zones during the mid-Neoproterozoic in the northern margin of the South China Block (Zheng et al. 2006).

Protolith of the Xuehe eclogite sample c81

Sample c81 has a very low content of very incompatible elements (Zr, Nb, and Th) that are normally enriched in the continental crust and, accordingly, the low Th/Yb ratios are more comparable to intra-oceanic supra-subduction zone basalts (either from island arc or back-arc settings) than tholeiitic continental basalts. The high Zr/Nb ratio of 18.0, the low Nb concentration of 0.92 ppm, and the negative Nb–Ta anomalies, appear to disapprove an OIB-type protolith (Spandler et al. 2004). The Ti/V ratio of ~22 is in the range for MORB and back-arc basalts (Shervais 1982). Nevertheless, back-arc basin spreading produces seafloor basalts with a composition that is largely indistinguishable from that produced at mid-ocean ridges (Stern 2010). The late-stage back-arc basin basalts (BABBs) can also exhibit a MORB-like pattern of trace element distribution (e.g., Pearce and Stern 2006). The clearly negative Nb anomalies cannot be attributed to any MORB. Moreover, the negative Pb anomaly is usually associated with a no Nb anomaly for MORBs. The positive Pb anomaly appears to favor a BABB origin for sample c81. Therefore, we tentatively propose that the c81 eclogite protolith is likely the later stage of BABBs in the tectonic setting of seafloor spreading. The highly primitive $^{143}Nd/^{144}Nd$ ratio ($\varepsilon_{Nd(0)}$ = +7.2) suggests a juvenile crustal origin for the c81 eclogite. Although zircon grains show no clear magmatic cores with oscillatory zonation, the presence of positive correlations between their Th and U contents of core or rim, clear Eu anomalies, steep LREE to HREE gradients, and no identification of metamorphic mineral inclusions, suggest that the c81 zircon ages reflect protolith formation. The Silurian to Devonian U–Pb ages are, therefore, proposed to record the timing of melt emplacement and crystallization, supporting the Paleotethyan crust model involving late Silurian/Early Devonian depleted mantle melting and the formation of the Paleotethyan oceanic crust (Wu et al. 2009; Cheng et al. 2009). The Xuehe eclogites, therefore, represent the coexistence of Neoproterozoic continental and Paleozoic oceanic crustal materials in the present Huwan shear zone.

Lu–Hf garnet constraints on the timing of peak metamorphism

A robust Lu–Hf garnet age requires that garnet behaved as a closed system over time and depends on how accurately the analyzed garnet separates reflect the complete garnet chemistry within the rock. The occurrence of the omphacite inclusions in both the core and rim (Fig. 3) of the garnets indicates that the overall garnet growth occurred during eclogite-facies metamorphism. Published estimates of the closing temperature of the garnet Lu–Hf system are > 630 °C (Skora et al. 2008), > 680 °C; (Scherer et al. 2000), > 800 °C (Schmidt et al. 2011), and approximately 1000 °C (Shu et al. 2013) and hence well above the peak temperatures of the Xuehe eclogite (< 580 °C). This, together with the preserved prograde chemical zoning in the garnet, discredits the interpretation of these ages as a re-equilibration or cooling age.

The variations in Lu–Hf amongst the garnet separates from the same sample could be caused by the mixing of different proportions of cores and rims between individual garnet separates, which can potentially produce high mean square of weighted deviates (MSWDs) (Kohn 2009) provided that the garnet grew over a period of several tens of Myr. The limited spread in parent/daughter ratios for the garnets (0.57–0.71 for c79 and 1.0–1.2 for c81) and the best-fit multi-fraction Lu–Hf isochron in a strict statistical sense (MSWD < 2.3 for 6-points or 5 degrees of freedom; Wendt and Carl 1991) imply limited age differences for different portions of the garnet, which were suppressed within the analytical resolution. The best-fit multi-fraction Lu–Hf isochron together with the limited variation in the $^{176}Lu/^{177}Hf$ suggest insignificant involvement of possibly unraveled older garnet cores in the bulk isotopic digestion. The good fit of the isochrons also indicates an insignificant effect of any Hf-bearing inclusions dissolved along with the garnet as well as retrograde reset of omphacite.

Inherited accessory minerals, particularly un-equilibrated zircon, can compromise the Lu-Hf age, by lowering the Lu/Hf and $^{176}Hf/^{177}Hf$ ratios of bulk garnet separates relative to those of pure garnet (Scherer et al. 2000). A selective tabletop-digestion procedure was applied to minimize the inherited effect. Including the bomb-digested whole rock for the continental eclogite (c79) yields a much lower initial $^{176}Hf/^{177}Hf$ value and an older apparent age (Fig. 5), clearly indicating that the zircon was not in initial isotopic equilibrium with the rest of the sample (i.e., inherited). This is consistent with the higher whole rock Zr concentrations (187 ppm for c79 vs. 16.7 ppm for c81) as well as the Neoproterozoic ages determined on zircons recovered from the continental eclogite. Collectively, these observations confirm that the Permian Lu–Hf ages reflect mineral growth during prograde/peak eclogite-facies metamorphism.

Ar–Ar age constraints on the timing of exhumation

The fairly flat Ar release patterns of the phengites indicate homogeneous Ar-isotopic composition released through the experiment, suggesting an undisturbed Ar-isotopic composition of the phengite (Fig. 8). Both Ar–Ar inverse isochrons yield atmospheric initial ratio, suggesting no significant excess Ar has been incorporated at or after the time of initial closure of the isotopic system in these phengites. Therefore, the integrated ages of both eclogites are interpreted to be geologically significant. The Triassic phengite Ar–Ar ages of the Xuehe eclogite are comparable to the phengite Ar–Ar ages of *ca*. 234 Ma (Webb et al. 1999) and *ca*. 243 Ma (Ye et al. 1994) for the Xiongdian eclogite to the west in this belt, and thus are interpreted to reflect a cooling age.

Coupled subduction and exhumation of the oceanic and continental crust

The occurrence of natural HP/UHP oceanic eclogites in subduction zones (e.g., Agard et al. 2009; Frezzotti et al. 2011; Plunder et al. 2012) indicates that at least parts of subducted oceanic crust can detach from the down-going slab and be exhumed back to the surface either due to its relatively lower density than the surrounding mantle, by being either less dehydrated, decoupled from the top part of the sinking slab at shallow depths (Cheng et al. 2013), or enveloped within low-density continental rocks (Cloos 1985; Hermann et al. 2000; Plunder et al. 2012). The consistent Permian Lu–Hf ages and Triassic Ar–Ar ages obtained for the Xuehe eclogites with distinct geochemically continental and oceanic affinities in this study imply coupled subduction and exhumation of oceanic and continental crustal materials in the Hong'an orogenic belt during the Permian and the Triassic, and the transitional time of oceanic to continental subduction could be traced back to *ca*. 260 Ma.

IMPLICATIONS

The coexistence of the Paleozoic oceanic crust and the Neoproterozoic continental crust and the coupled subduction of oceanic and continental crust during the Carboniferous and the Permian, and exhumation during the Triassic, registered in the eclogites from the Huwan shear zone lead us to propose that a Neoproterozoic micro-continental crust was separated from the main South China Block by the Paleo-Tethys Ocean (Fig. 9). The closure of an oceanic basin (Shangdan ocean?) to the north of the micro-continent was generated by the progressive northward subduction of the Paleotethyan oceanic lithosphere. The micro-continental crust of the northern South China Block and the coexisting oceanic crust were both subducted northward beneath the North China Block and was subjected to HP eclogite-facies metamorphism at *ca*. 310 Ma. The ultimate convergence of the South China Block and the North China Block led to the subduction of the Paleotethyan oceanic crust and the collision between the two blocks. During this process some of the underplated/exhumed Carboniferous eclogites were partially incorporated into the subduction channel and exhumed until the entrance of buoyant continental material into the subduction zone during the Permian. This model predicts two distinct evolution paths for the Huwan eclogite: (1) some eclogites have experienced eclogite-facies metamorphism in two orogenic cycles during the Carboniferous and the Permian; (2) the others have been involved only in a single subduction loop during the Permian and suffered a single eclogite-facies metamorphism (Fig. 9e) probably due to involvement of the edge of the obduction into the subduction channel.

Recently, an increasing number of observations from orogenic belts have been suggesting polyphase-subduction or multiple eclogite-facies metamorphism within a single unit or as two orogenic cycles (e.g., Rubatto et al. 2011; Herwartz et al. 2011; Root and Corfu 2012; Kirchenbaur et al. 2012). These observations appear to be in accordance with multiple subduction–exhumation cycles for individual rock units by tectonic models (Gerya et al. 2002; Brueckner 2006). The Xuehe eclogites from the Huwan shear zone appear to suggest another case of two loops of high-pressure orogenic cycles in a single orogen. However, the coupled single subduction model and the diachronous subduction and exhumation scenarios primarily advance from the existing geochemical data and chronometric results, further direct and indirect observations from other aspects, such as related sedimentation and magmatism, and field geology, are highly required to better our understanding of the tectonic evolution of the oceanic to continental subduction and exhumation in the Hong'an orogenic belt.

ACKNOWLEDGEMENTS

We thank S. Andrew DuFrane and Chao Zhang for helping the isotope analyses at Pullman. Valuable discussions with Wei Lin, Hafiz Ur Rehman, Marco Scambelluri, and Ethan Baxter improved interpretations of our data. Chemical analysis was funded by the National Natural Science Foundation of China (41373005). Field work was funded by the Fundamental Research Funds for the Central Universities. We thank Edward Ghent for his editorial managing of the manuscript and for a valuable review that steered the presentation of the manuscript in the right direction. We are grateful to Timothy Nesheim and Alex Zirakparvar for their thorough and constructive comments to the manuscript.

REFERENCES CITED

Agard, P., Yamato, P., Jolivet, L., and Burov, E. (2009) Exhumation of oceanic blueschists and eclogites in subduction zones: timing and mechanisms. Earth Science Reviews, 92, 53–79.

Ague, J.J., and Carlson, W.D. (2013) Metamorphism as Garnet Sees It: The Kinetics of Nucleation and Growth, Equilibration, and Diffusional Relaxation. Elements, 9, 439–445.

Ayers, J.C., Dunkle, S., Gao, S., and Miller, C.F. (2002) Constraints on timing of peak and retrograde metamorphism in the Dabie Shan ultrahigh-pressure metamorphic belt, east-central China, using U–Th–Pb dating of zircon and monazite. Chemical Geology, 186, 315–331.

Baldwin, S.L., Webb, L.E., and Monteleone, B.D. (2008) Late Miocene coesite–eclogite exhumed in the Woodlark Rift. Geology, 36, 735–738.

Baxter, E.F., and Caddick, M.J. (2013) Garnet growth as a proxy for progressive subduction zone dehydration. Geology, 41, 643–646.

Baxter, E.F., and Scherer, E.E. (2013) Garnet Geochronology: Timekeeper of Tectonometamorphic Processes. Elements, 9, 433–438.

Berger, J., Féménias, O., Ohnenstetter, D., Bruguier, O., Plissart, G.,Mercier, J.C.C., and Demaiffe, D. (2010) New occurrence of UHP eclogites in Limousin (French Massif Central): Age, tectonic setting and fluid-rock interactions. Lithos, 118, 365–382.

Bouvier, A., Vervoort, J.D., and Patchett, P.J. (2008) The Lu–Hf and Sm–Nd isotopic composition of CHUR: constraints from unequilibrated chondrites and implications for the bulk composition of terrestrial planets. Earth and Planetary Science Letters, 273, 48–57.

Brouwer, F.M., Groen, M., Nebel, O., Wijbrans, J.R., Qiu, H., Yang, Q., Zhao, L.H., and Wu, Y.B. (2011) Coherence of the Dabie Shan UHPM Terrane Investigated by Lu–Hf and $^{40}Ar/^{39}Ar$ Dating of Eclogites. In: Dobrzhinetskaya, L., (Ed.), Ultrahigh-Pressure Metamorphism. Elsevier, pp. 325–357.

Brueckner, H.K. (2006) Dunk, dunkless and re-dunk tectonics: A model for metamorphism, lack of metamorphism, and repeated metamorphism of HP/UHP terranes. International Geology Review, 48, 978–995.

Bryant, D.L., Ayers, J.C., Gao, S., Miller, C.F., and Zhang, H. (2004) Geochemical, age, and isotopic constraints on the location of the Sino-Korean/South China Suture and evolution of the Northern Dabie Complex, east central China. Geological Society of America Bulletin, 116, 698–717.

Chen, J., and Jahn, B.-m. (1998) Crustal evolution of southeastern China: Nd and Sr isotopic evidence. Tectonophysics, 284, 101–133.

Cheng, H., King, R.L., Nakamura, E., Vervoort, J.D., Zheng, Y.F., Ota, T., Wu, Y.B., Kobayashi, K., and Zhou, Z.Y. (2009) Transitional time of oceanic to continental subduction in the Dabie orogen: constraints from U–Pb, Lu–Hf, Sm–Nd and Ar–Ar multichronometric dating. Lithos, 101, 327–342.

Cheng, H., King, R.L., Nakamura, E., Vervoort, J.D., and Zhou, Z. (2008) Coupled Lu–Hf and Sm–Nd geochronology constrains garnet growth in ultra-high-pressure eclogites from the Dabie orogen. Journal of Metamorphic Geology, 26, 741–758.

Cheng, H., DuFrane, S.A., Vervoort, J.D., Nakamura, E., Zheng, Y.F., and Zhou, Z.Y. (2010) Protracted oceanic subduction prior to continental subduction: new Lu–Hf and Sm–Nd geochronology of oceanic-type high-pressure eclogite in the western Dabie orogen. American Mineralogist, 95, 1214–1223.

Cheng, H., Zhang, C., Vervoort, D.J., Wu, Y.B., Zheng, Y.F., Zheng, S., and Zhou, Z.Y. (2011) New Lu–Hf geochronology constrains the onset of continental subduction in the Dabie orogen. Lithos, 121, 41–54.

Cheng, H., Zhang, C., Vervoort, J.D., Li, X.H., Li, Q.L., Wu, Y.B., and Zheng, S. (2012) Timing of eclogite facies metamorphism in the North Qinling by U–Pb and Lu–Hf geochronology. Lithos, 136–139, 46–59.

Cheng, H., Zhang, C., Vervoort, J.D., and Zhou, Z.Y. (2013) New Lu-Hf and Sm-Nd geochronology constrains the subduction of oceanic crust during the Carboniferous-Permian in the Dabie orogen. Journal of Asian Earth Sciences, 63, 139–150.

Cloos, M. (1985) Thermal evolution of convergent plate margins: thermal modeling and reevaluation of isotopic Ar-ages for blueschists in the Franciscan Complex, California. Tectonics, 4, 421–433.

Depaolo, D.J., and Wasserburg, G.J. (1979) Neodymium isotopes in flood basalts from the Siberian Platform and inferences about their mantle sources. Proceedings of the National Academy of Sciences of the United States of America, 76, 3056–3060.

Dodson, M.H. (1973) Closure temperature in cooling geochronological and petrological systems. Contributions to Mineralogy and Petrology, 40, 259–264.

Duchêne, S., Blichert-Toft, J., Luai,s B., Télouk, P., Lardeaux, J.M., and Albarède, F. (1997) The Lu–Hf dating of garnets and the ages of the Alpine high-pressure metamorphism. Nature, 387, 586–589.

Ernst, W.G. (2005) Alpine and Pacific styles of Phanerozoic mountain building: subduction-zone petrogenesis of continental crust. Terra Nova, 17, 165–188.

Frezzotti, M.L., Selverstone, J., Sharp, Z.D., and Compagnoni, R. (2011) Carbonate dissolution during subduction revealed by diamond-bearing rocks from the Alps. Nature Geoscience, 4, 703–706.

Fu, B., Zheng, Y.-F., and Touret, J.L.R. (2002) Petrological, isotopic and fluid inclusion studies of eclogites from Sujiahe, NW Dabie Shan (China). Chemical Geology, 187, 107–128.

Gao, S., Qiu, Y., Ling, W., McNaughton, N.J., Zhang, B., Zhang, G., Zhang, Z., Zhong, Z., and Suo, S. (2002) SHRIMP single zircon U–Pb geochronology of eclogites from Yingshan and Xiongdian. Earth Science: Journal of China University of Geosciences, 27, 558–564 (in Chinese with English abstract).

Gerya, T., Stockhert, B., and Perchuk, A. (2002) Exhumation of high-pressure metamorphic rocks in a subduction channel: A numerical simulation. Tectonics, 21(6), T10566, doi:10.1029/2002TC001406.

Hacker, B.R., Ratschbacher, L., Webb, L., Ireland, T., Walker, D., and Dong, S. (1998) U/Pb zircon ages constrain the architecture of the ultrahigh-pressure Qinling-Dabie Orogen, China. Earth and Planetary Science Letters, 161, 215–230.

Hacker, B.R., Ratschbacher, L., Webb, L., McWilliams, M.O., Ireland, T., Calvert, A., Dong, S.W., Wenk, H.R., and Chateigner, D. (2000) Exhumation of ultrahigh-pressure continental crust in east central China: Late Triassic–Early Jurassic tectonic unroofing. Journal of Geophysical Research-Solid Earth, 105, 13339–13364.

Hermann, J., Müntener, O., and Scambelluri, M. (2000) The importance of serpentinite mylonites for subduction and exhumation of oceanic crust. Tectonophysics, 327, 225–238.

Herwartz, D., Nagel, T.J., Münker, C., Scherer, E.E., and Froitzheim, N. (2011) Tracing two orogenic cycles in one eclogite sample by Lu–Hf garnet chronometry. Nature Geoscience, 4, 178–183.

Holland, T.J.B., and Powell, R. (1998) An internally consistent thermodynamic data set for phases of petrological interest. Journal of Metamorphic Geology, 16, 309–343.

Hu, Z.C., Liu, Y.S., Chen, L., Zhou, L., Li, M., Zong, K.Q., Zhu, L.Y., and Gao, S. (2011) Contrasting Matrix Induced Elemental Fractionation in NIST SRM and Rock Glasses during Laser Ablation ICP-MS Analysis at High Spatial Resolution, Journal of Analytical Atomic Spectrometry, 26, 425–430.

Jahn, B.M. (1998) Geochemical and isotopic characteristics of UHP eclogites and ultramafic rocks of the Dabie orogen: implications for continental subduction and collisional tectonics. In: Hacker, B., Liou, J.G. (Eds.), When continents collide: geodynamics and geochemistry of ultrahigh-pressure rocks. Kluwer Acad. Publishers, Dordrecht, The Netherlands.

Jahn, B.M., Liu, X.C., Yui, T.F., Morin, N., and Bouhnik-Le Coz, M. (2005) High-pressure/ultra-high-pressure eclogites from the Hong'an Block, East-Central China: geochemical characterization, isotope disequilibrium and geochronological controversy. Contributions to Mineralogy and Petrology, 149, 499–526.

Jian, P., Yang, W., and Li, Z. (1997) Isotopic geochronological evidence for the Caledonian Xiongdian eclogite in the western Dabie mountains, China. Acta Geologica Sinica, 10, 455–465.

Jian, P., Liu, D., Yang, W., and Williams, I.S. (2000) Petrographical study of zircons and SHRIMP dating of the Caledonian Xiongdian eclogite, Northwestern Dabie Mountains. Acta Geologica Sinica, 74, 259–264.

Kirchenbaur, M., Pleuger, J., Jahn-Awe, S., Nagel, T.J., Froitzheim, N., Fonseca, R.O.C., and Münker, C. (2012) Timing of high-pressure metamorphic events in the Bulgarian Rhodopes from Lu–Hf garnet geochronology. Contributions to Mineralogy and Petrology, 163:897–921.

Kohn, M.J. (2009) Models of garnet differential geochronology. Geochimica et Cosmochimica Acta, 73, 170–182.

Krogh-Ravna, E.J. (2000) The garnet-clinopyroxene Fe^{2+}–Mg geothermometer: an updated calibration. Journal of Metamorphic Geology, 18, 21–219.

Krogh-Ravna, E.J., and Terry, M.P. (2004) Geothermobarometry of UHP and HP eclogites and schists–an evaluation of equilibria among garnet–clinopyroxene–kyanite–phengite–coesite/quartz. Journal of Metamorphic Geology, 22, 579–592.

Kröner, A., Zhang, G.W., and Sun, Y. (1993) Granulites in the Tongbai area, Qinling belt, China: geochemistry, petrology, single zircon geochronology, and implications for the tectonic evolution of Eastern Asia. Tectonics, 12, 245–255.

Lapen, T.J., Johnson, C.M., Baumgartner, L.P., Mahlen, N.J., Beard, B.L., and Amato, J.M. (2003) Burial rates during prograde metamorphism of an ultra-high-pressure terrane: an example from Lago di Cignana, western Alps, Italy. Earth and Planetary Science Letters, 215, 57–72.

Lebas, M.J. (1989) Nephelinitic and Basanitic Rocks. Journal of Petrology, 30, 1299–1312.

Li, S., Huang, F., Nie, Y., Han, W., Long, C., Li, H., Zhang, S., and Zhang, Z. (2001) Geochemical and Geochronological constraints on the suture location between the North and South China blocks in the Dabie orogen, central China. Physics and Chemistry of the Earth (A), 26, 655–672.

Liu, X.C., Wei, C., Li, S., Dong, S., and Liu, J. (2004) Thermobaric structure of a traverse across western Dabieshan: implications for collision tectonics between the Sino-Korean and South China cratons. Journal of Metamorphic Geology, 22, 361–379.

Liu, X.C., Jahn, B.-M., Dong, S., Lou, Y., and Cui, J. (2008a) High-pressure metamorphic rocks from Tongbaishan, central China: U–Pb and $^{40}Ar/^{39}Ar$ age constraints on the provenance of protoliths and timing of metamorphism. Lithos, 105, 301–318.

Liu, Y.S., Hu, Z.C., Gao, S., Günther, D., Xu, J., Gao, C.G., and Chen, H.H. (2008b) In situ analysis of major and trace elements of anhydrous minerals by LA-ICP-MS without applying an internal standard. Chemical Geology, 257, 34–43.

Liu, X.C., Wu, Y.B., Gao, S., Wang, J., Peng, M., Gong, H.J., Liu, Y.S., and Yuan, H.L. (2010) Zircon U–Pb and Hf evidence for coupled subduction of oceanic and continental crust during the Carboniferous in the Huwan shear zone, western Dabie orogen, central China. Journal of Metamorphic Geology, 29, 233–249.

Ludwig, K.R. (2008) User Manual for Isoplot/Ex Version 3.70. A Geochronological ToolKit for Microsoft Excel. Berkeley Geochronology Center Special Publication No. 2. p. 77.

Lugmair, G.W., and Marti, K. (1978) Lunar initial ^{143}Nd/^{144}Nd: differential evolution of the lunar crust and mantle. Earth and Planetary Science Letters, 39, 349–357.

Massonne, H.J. (2013) Constructing the Pressure–Temperature Path of Ultrahigh-Pressure Rocks. 9, 267–272.

Mattauer, M., Matte, P., Malavieille, J., Tapponnier, P., Maluski, H., Xu, Z.Q., Lu, Y.L., and Tang, Y.Q. (1985) Tectonics of the Qinling belt: build-up and evolution of eastern Asia. Nature, 317, 496–500.

Meng, Q.R., and Zhang, G.W. (1999) Timing of collision of the North and South China blocks: controversy and reconciliation. Geology, 27, 123–126.

Mulcahy, S.R., King, R.L., and Vervoort, J.D. (2009) Lawsonite Lu–Hf geochronology: A new geochronometer for subduction zone processes. Geology, 37, 987–990.

O'Brien, P.J. (2001) Subduction followed by Collision: Alpine and Himalayan examples. In: Rubie, D.C. & van der Hilst, R. (eds), Processes and Consequences of Deep Subduction, Physics of the Earth and Planetary Interiors, 127, 277–291.

Otamendi, J.E., Rosa J.D., Douce A.E.P., and Castro, A. (2002) Rayleigh fractionation of heavy rare earths and yttrium during metamorphic garnet growth. Geology, 30, 159–162.

Pearce, J.A., and Stern, R.J. (2006) The origin of back-arc basin magmas: trace element and isotope perspectives. In: Christie, D.M., Fisher, C.R., Lee, S.-M., Givens, S. (Eds.), Back-arc Spreading Systems: Geological, Biological, Chemical and Physical Interactions: American Geophysical Union Geophysical Monograph, 166, pp. 63–86.

Peters, T.J., Ayers, J.C., Gao, S., and Liu, X.M. (2013) The origin and response of zircon in eclogite to metamorphism during the multi-stage evolution of the Huwan Shear Zone, China:

Insights from Lu–Hf and U–Pb isotopic and trace element geochemistry. Gondwana Research, 23,726–747.

Plunder, A., Agard, P., Dubacq, B., Chopin, C., and Bellanger, M. (2012) How continuous and precise is the record of P-T paths? Insights from combined thermobarometry and thermodynamic modelling into subduction dynamics (Schistes Lustres, W. Alps). Journal of Metamorphic Geology, 30, 323–346.

Ratschbacher, L., Franz, L., Enkelmann, E., Jonckheere, R., Pörschke, A., Hacker, B.R., Dong, S., and Zhang, Y. (2006) The Sino-Korean-South China suture, the Huwan detachment, and the Paleozoic-Tertiary exhumation of (ultra)high-pressure rocks along the Tongbai-Xinxian-Dabie Mountains. Special Paper 403: Ultrahigh-pressure metamorphism: Deep continental subduction, 403, 45–75.

Root, D., and Corfu, F. (2012) U–Pb geochronology of two discrete Ordovician high-pressure metamorphic events in the Seve Nappe Complex, Scandinavian Caledonides. Contributions to Mineralogy and Petrology, 163, 769–788.

Rubatto, D., and Hermann, J., 2007. Experimental zircon/melt and zircon/garnet trace element partitioning and implications for the geochronology of crustal rocks. Chemical Geology, 241, 38–61.

Rubatto, D., Regis, D., Hermann, J., Boston, K., Engi, M., Beltrando, M., and McAlpine, S.R.B. (2011) Yo-yo subduction recorded by accessory minerals in the Italian Western Alps. Nature Geoscience, 4, 338–342.

Rudnick, R.L., and Gao, S. (2003) Composition of the continental crust. In: Rudnick, R.L. (Ed.), The Crust. : Treatise on Geochemistry, 3. Elsevier-Pergamon, Oxford, pp. 1–64.

Scherer, E.E., Münker, C., and Mezger, K. (2001) Calibration of the lutetium-hafnium clock. Science, 293, 683–687.

Scherer, E.E., Cameron, K.L., and Blichert-Toft, J. (2000) Lu–Hf garnet geochronology: closure temperature relative to the Sm–Nd system and the effects of trace mineral inclusions. Geochimica et Cosmochimica Acta, 64, 3413–3432.

Schmidt, A., Mezger, K., Scherer, E.E., Xiao, Y.L., Hoefs, J., and Brey, G.P. (2008) Rapid eclogitisation of the Dabie–Sulu UHP terrane: constraints from Lu–Hf garnet geochronology. Earth and Planetary Science Letters, 273, 203–213.

Schmidt, A., Mezger, K., and O'Brien, P.J. (2011) The time of eclogite formation in the ultrahigh pressure rocks of the Sulu terrane. Constraints from Lu–Hf garnet geochronology. Lithos, 125, 743–756.

Shervais, J.W. (1982) Ti–V plots and the petrogenesis of modern and ophiolitic lavas. Earth and Planetary of Science Letters, 59, 101–118.

Shu, Q., Brey, G.P., Gerdes, A., and Höfer, H.E. (2013) Geochronological and geochemical constraints on the formation and evolution of the mantle underneath the Kaapvaal craton: Lu–Hf and Sm–Nd systematics of subcalcic garnets from highly depleted peridotites. Geochimica Cosmochimica Acta, 113, 1–20.

Skora, S., Baumgartner, L.P., Mahlen, N.J., Johnson, C.M., Pilet, S., and Hellebrand, E. (2006) Diffusion-limited REE uptake by eclogite garnets and its consequences for Lu–Hf and Sm–Nd geochronology. Contributions to Mineralogy and Petrology, 152, 703–720.

Skora, S., Baumgartner, L.P., Mahlen, N.J., Lapen, T.J., Johnson, C.M., and Bussy, F. (2008) Estimation of a maximum Lu diffusion rate in a natural eclogite garnet. Swiss Journal of Geosciences, 101, 637–650.

Smit, M.A., Scherer, E.E., and Mezger, K. (2013) Lu–Hf and Sm–Nd garnet geochronology: Chronometric closure and implications for dating petrological processes. Earth and Planetary Science Letters, 381, 222–233.

Söderlund, U., Patchett, P.J., Vervoort, J.D., and Isachsen, C.E. (2004) The ^{176}Lu decay constant determined by Lu–Hf and U–Pb isotope systematics of Precambrian mafic intrusions. Earth and Planetary Science Letters, 219, 311–324.

Spandler, C., Hermann, J., and Rubatto, D. (2004) Exsolution of thortveitite, yttrialite, and xenotime during low-temperature recrystallization of zircon from New Caledonia, and their significance for trace element incorporation in zircon. American Mineralogist, 89, 1795–1806.

Spear, F.S., and Selverstone, J. (1983) Quantitative P-T paths from zoned minerals: theory and tectonic applications. Contributions to Mineralogy and Petrology, 83, 348–357.

Stern, R.J. (2010) The anatomy and ontogeny of modern intra-oceanic arc systems. Geological Society, Special Publication, 338, 7–34.

Sun, S.-S., and McDonough, W.F. (1989) Chemical and isotopic systematics of oceanic basalts: implications for mantle composition and processes. In Saunders, A.D., Norry, M.J. (Eds.), Magmatism in Ocean Basins. Geological Society of London Special Publication, No. 42. pp. 313–345.

Sun, W., Williams, I.S., and Li, S. (2002) Carboniferous and Triassic eclogites in the western Dabie Mountains, east-central China: evidence for protracted convergence of the North and South China blocks. Journal of Metamorphic Geology, 20, 873–886.

Vervoort, J.D., Patchett, P.J., Söderlund, U., and Baker, M. (2004) Isotopic composition of Yb and the determination of Lu concentrations and Lu/Hf ratios by isotope dilution using

MC-ICPMS, Geochemistry Geophysics Geosystems, 5, Q11002, doi:10.1029/2004GC000721.

Webb, L., Hacker, B., Ratschbacher, L., McWilliams, M., and Dong, S. (1999) Thermochronologic constraints on deformation and cooling history of high and ultrahigh-pressure rocks in Qinling–Dabie orogen, eastern China. Tectonics, 18, 621–638.

Wendt, I., and Carl, C. (1991) The statistical distribution of the mean squared weighted deviation. Chemical Geology, 86, 275–285.

Wiedenbeck, M., Hanchar, J.M., Peck, W.H., Sylvester, P., Valley, J., White-house, M., Kronz, A., Morishita, Y., and Nasdala, L. (2004) Further characterization of the 91500 zircon crystal. Geostandards and Geoanalysis, 28, 9–39.

Wu, Y.-B., Hanchar, J.M., Gao, S., Sylvester, P.J., Tubrett, M., Qiu, H.N., Wijbrans, J.R., Brouwer, F.M., Yang, S.H., Yang, Q.J., Liu, Y.S., and Yuan, H.L. (2009) Age and nature of eclogites in the Huwan shear zone, and the multi-stage evolution of the Qinling-Dabie-Sulu orogen, central China. Earth and Planetary Science Letters, 277, 345–354.

Wu, Y.-B., and Zheng, Y.-F. (2013) Tectonic evolution of a composite collision orogen: An overview on the Qinling–Tongbai–Hong'an–Dabie–Sulu orogenic belt in central China. Gondwana Research, 23, 1402–1428.

Xu, B., Grove, M., Wang, C., Zhang, L., and Liu, S. (2000) $^{40}Ar/^{39}Ar$ thermochronology from the northwestern Dabie Shan: constraints on the evolution of Qinling–Dabie orogenic belt, east-central China. Tectonophysics, 322, 279–301.

Ye, B.D., Jiang, P., Xu, J., Cui, F., Li, Z., and Zhang, Z. (1993) The Sujiahe terrane collage belt and its constitution and evolution along the northern hillside of the Tongbai–Dabie orogenic belt. Press of China University of Geoscience, Wuhan, pp.1–81 (in Chinese with English abstract).

_____ (1994) Timing of the Sujiahe group in the Tongbai-Dabie orogenic belt, in Chen, H., ed., Research of isotope geochemistry: Hangzhou, Zhejiang University Press, pp. 175–186.

Zheng, Y.F., Zhao, Z.F., Wu, Y.B., Zhang, S.B., Liu, X.M., and Wu, F.Y. (2006) Zircon U–Pb age, Hf and O isotope constraints on protolith origin of ultrahigh-pressure eclogite and gneiss in the Dable orogen. Chemical Geology, 231, 135–158.

Zheng, Y.-F. (2012) Metamorphic chemical geodynamics in continental subduction zones. Chemical Geology, 328, 5–48.

Zhou, G., Liu, Y.J., Eide, E.A., Liou, J.G., and Ernst, W.G. (1993) High pressure low temperature metamorphism in northern Hubei Province, central China. Journal of Metamorphic Geology, 11, 561–574.

Zirakparvar, N.A., Baldwin, S.L., and Vervoort, J.D. (2011) Lu–Hf garnet geochronology applied to plate boundary zones: Insights from the (U)HP terrane exhumed within the Woodlark Rift. Earth and Planetary Science Letters, 309, 56–66.

Figure Captions

FIGURE 1. Simplified geologic map of the Huwan shear zone **(b)** in Hong'an orogenic belt **(a)**; compiled from maps by Ye et al. (1993) and Liu (2004); (c-f) Field occurrence of the Xuehe eclogite within gneiss.

FIGURE 2. Trace-element data for the Xuehe eclogite: **(a)** chondrite-normalized REE patterns, showing distinct patterns; **(b)** N-MORB-normalized spider diagram; **(c)** The Nd isotope diagram

for the Xuehe eclogite. The Sm–Nd data for eclogites of the Dabie–Sulu (Jahn 1995; Cheng et al. 2008; Schmidt et al. 2008) are also shown for comparison; **(d)** $\varepsilon_{Nd(t)}$ *vs*. time (Ga) for the Xuehe eclogite. Normalizing values follow Sun and McDonough (1989).

FIGURE 3. Photomicrographs of the Xuehe eclogite and backscattered-electron images and rim-to-rim major-element compositional zoning profiles of representative garnet porphyroblasts. **(a-d)** The continental-type eclogite sample (c79); **(e-h)** The oceanic-type eclogite sample (c81). Ep − epidote; Grt − garnet; Omp − omphacite; Phen − phengite; Qtz − quartz.

FIGURE 4. Peak P–T estimates for the Xuehe eclogite. Calculated reaction equilibria are: Fe^{2+}/Mg exchange between garnet and omphacite (Krogh-Ravna 2000), celadonite + pyrope = grossular + muscovite + diopside (Krogh-Ravna and Terry 2004). The latter are plotted according to the calibrations of Holland and Powell (1998, latest updated dataset). The temperatures were estimated by THERMOCALC3.33. The minimum and maximum limits of the P–T estimates defined by intersections of calculated reaction equilibria are noted in solid squares. Error ellipses of the average P–T calculations by the *av*PT (Holland and Powell 1998) are reported with 1σ uncertainty.

FIGURE 5. Lu–Hf isochron plots for samples **(a)** c79 and **(b)** c81. Grt − garnet, Omp − omphacite, WR.sav – whole rock by Savillex-digestion, WR.bomb – whole rock by Bomb-digestion. Error bars are significantly smaller than the size of the symbols. MSWD − mean square of weighted deviates.

FIGURE 6. **(a)** CL images and Tera–Wasserburg concordia diagrams (uncorrected for common Pb) for the Xuehe eclogite. Data-point error ellipses are shown at the 1σ confidence level. The probability density function and histogram include only concordant zircon ages (blue circles) of the oceanic eclogite. **(b)** Chondrite normalized REE patterns of zircons.

FIGURE 7. Correlation between Th and U of zircons from sample c81 **(a)** and c79 **(b)**. Error bars are significantly smaller than the size of the symbols.

FIGURE 8. Ar–Ar age spectra and inverse isochrons for phengites within the continental eclogite **(a, b)** and the oceanic eclogites **(c, d)**, respectively. Errors are reported with 1σ uncertainty. The plateau are defined by 65% and 100% of ^{39}Ar fractions released for phengites from the continental eclogite and the oceanic eclogite, respectively. Solid symbols, defining the line, were used to calculate the isochron, open symbols were not used in the calculation. See text for details.

FIGURE 9. Cartoon illustrating the tectonic evolution of the Huwan shear zone. **(a)** Closure of the Shangdan basin and the opening of a Paleo-Tethys Ocean to the south of a micro-continent. **(b)** Northward subduction of the Paleo-Tethys oceanic lithosphere entrained some early oceanic and continental fragments. **(c)** Termination of oceanic subduction and beginning of continental subduction, followed by the exhumation of (ultra-)high-pressure rocks. **(d)** Successive doming and magmatic intrusion and extension exposing the present coexisting oceanic-type and continental-type high-pressure rocks. **(e)** Enlarged coexisting oceanic-type and continental-type eclogites that experimented single or two loops of high-pressure metamorphism.

Table Captions

TABLE 1 Chemical compositions of the Xuehe eclogite.

TABLE 2 Representative major-element data of the garnets, omphacites, phengites, epidotes and amphiboles

TABLE 3 Garnet REE data obtained by LA-ICP-MS for the Xuehe eclogite.

TABLE 4 Lu–Hf isotope data for the Xuehe eclogite.

Appendix 1 (Supplementary Table 5) Zircon U–Pb isotopic data obtained by LA-ICP-MS for zircons from Xuehe eclogites.

Appendix 2 (Supplementary Table 6) LA-ICP-MS trace element analyses of zircons from Xuehe eclogites.

Appendix 3 (Supplementary Table 7) $^{40}Ar/^{39}Ar$ step heating data for phengites from Xuehe eclogites.

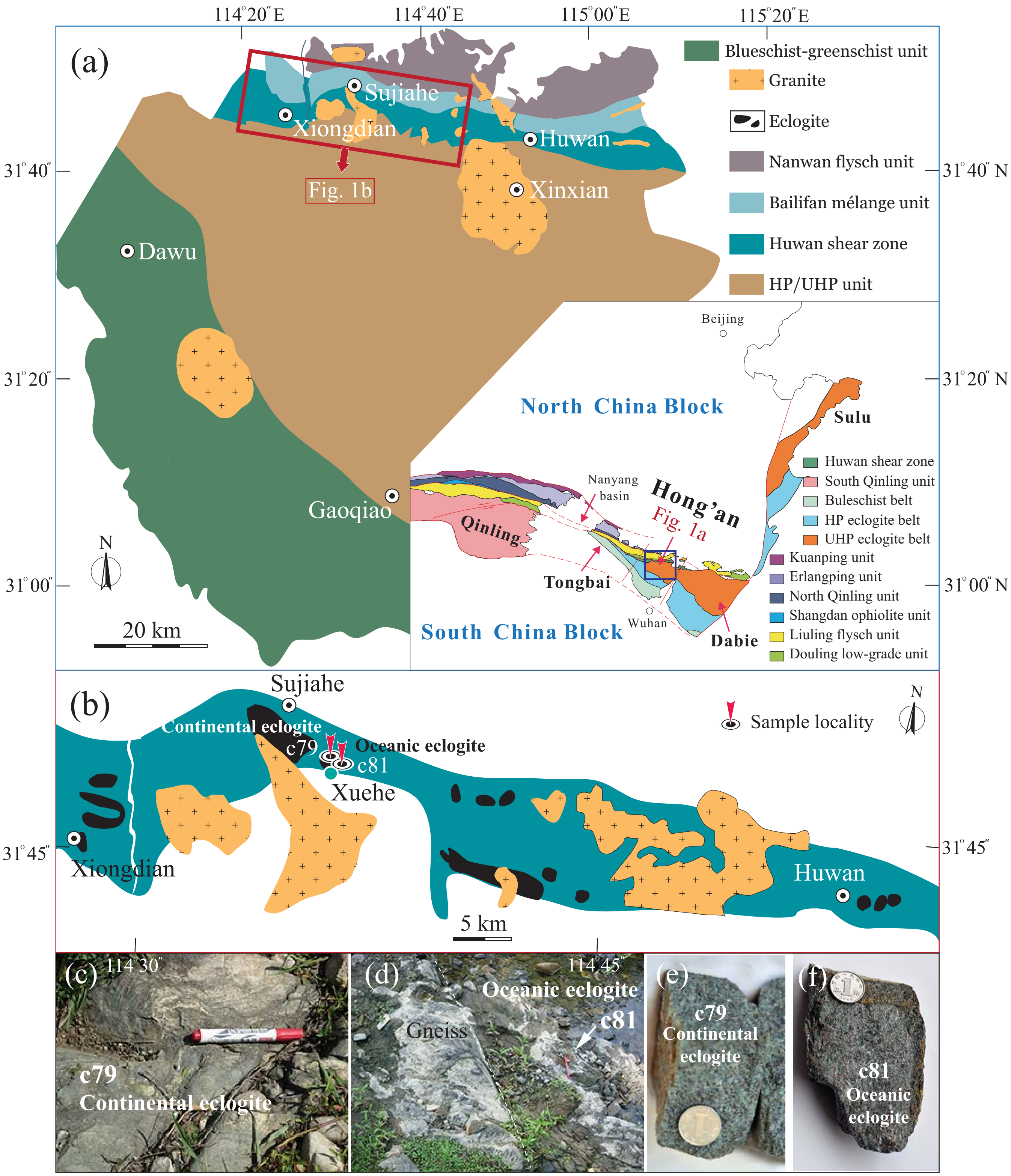

Figure 1

Cheng et al., 2014

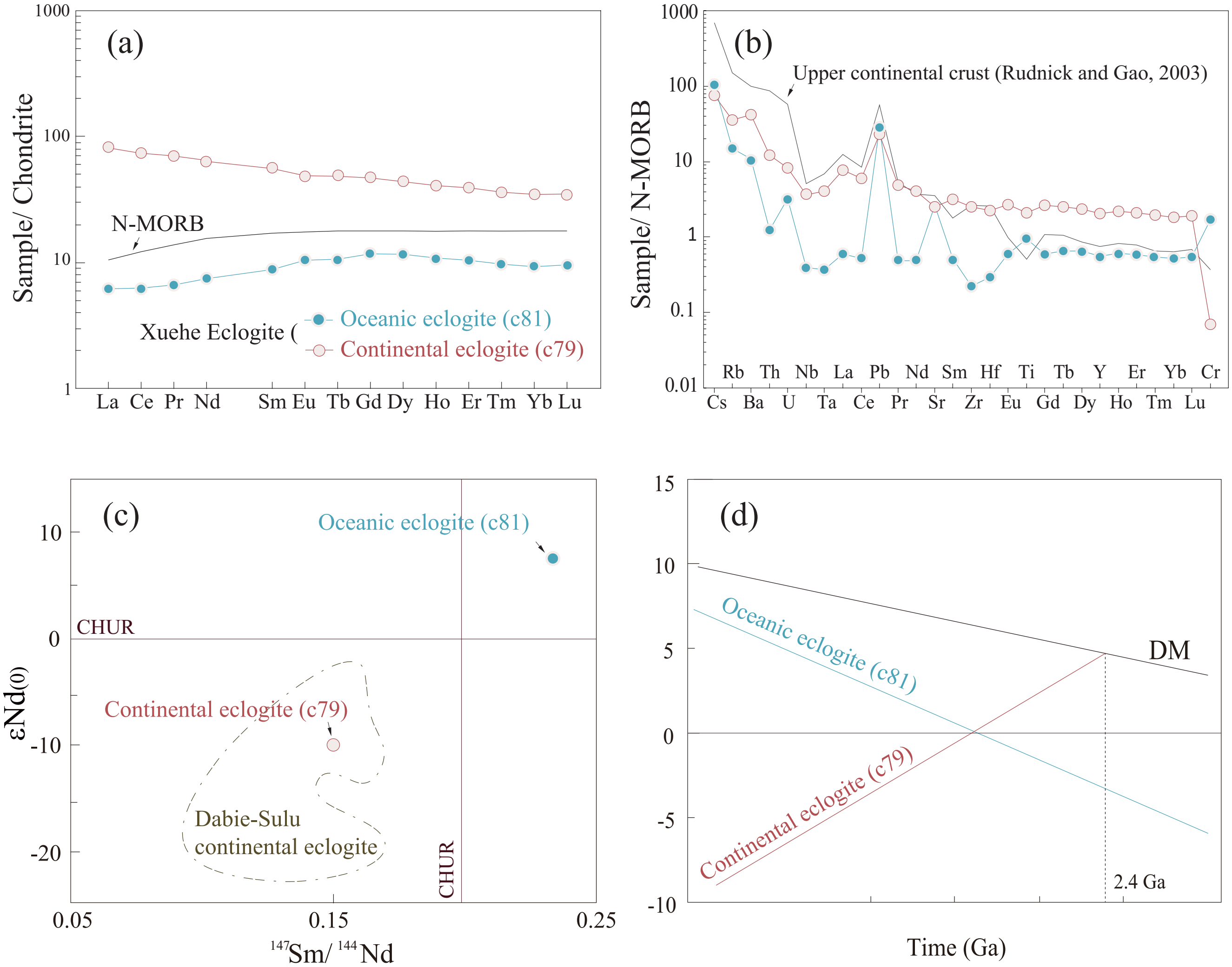

Figure 2

Cheng et al., 2014

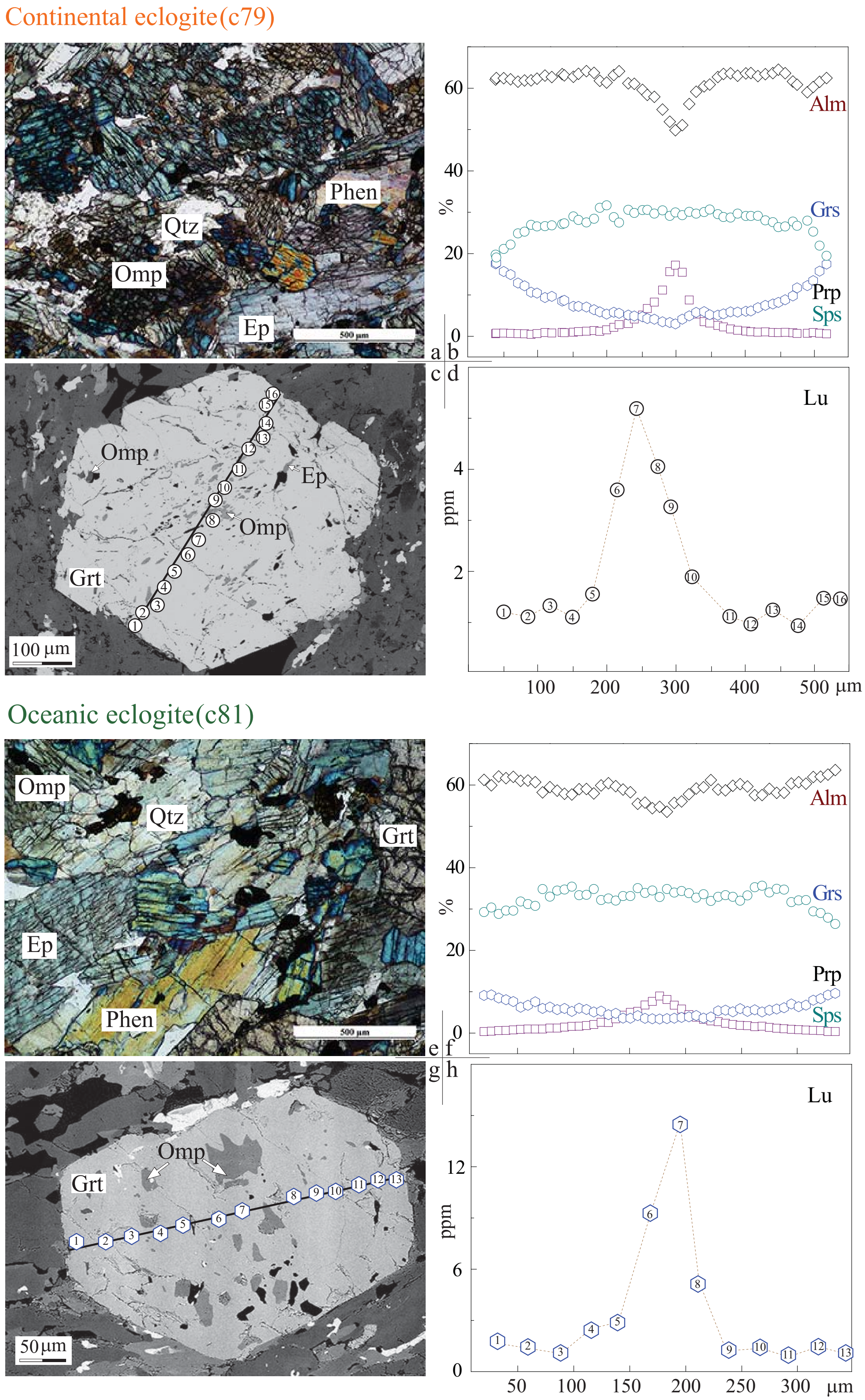

Figure 3

Cheng et al., 2014

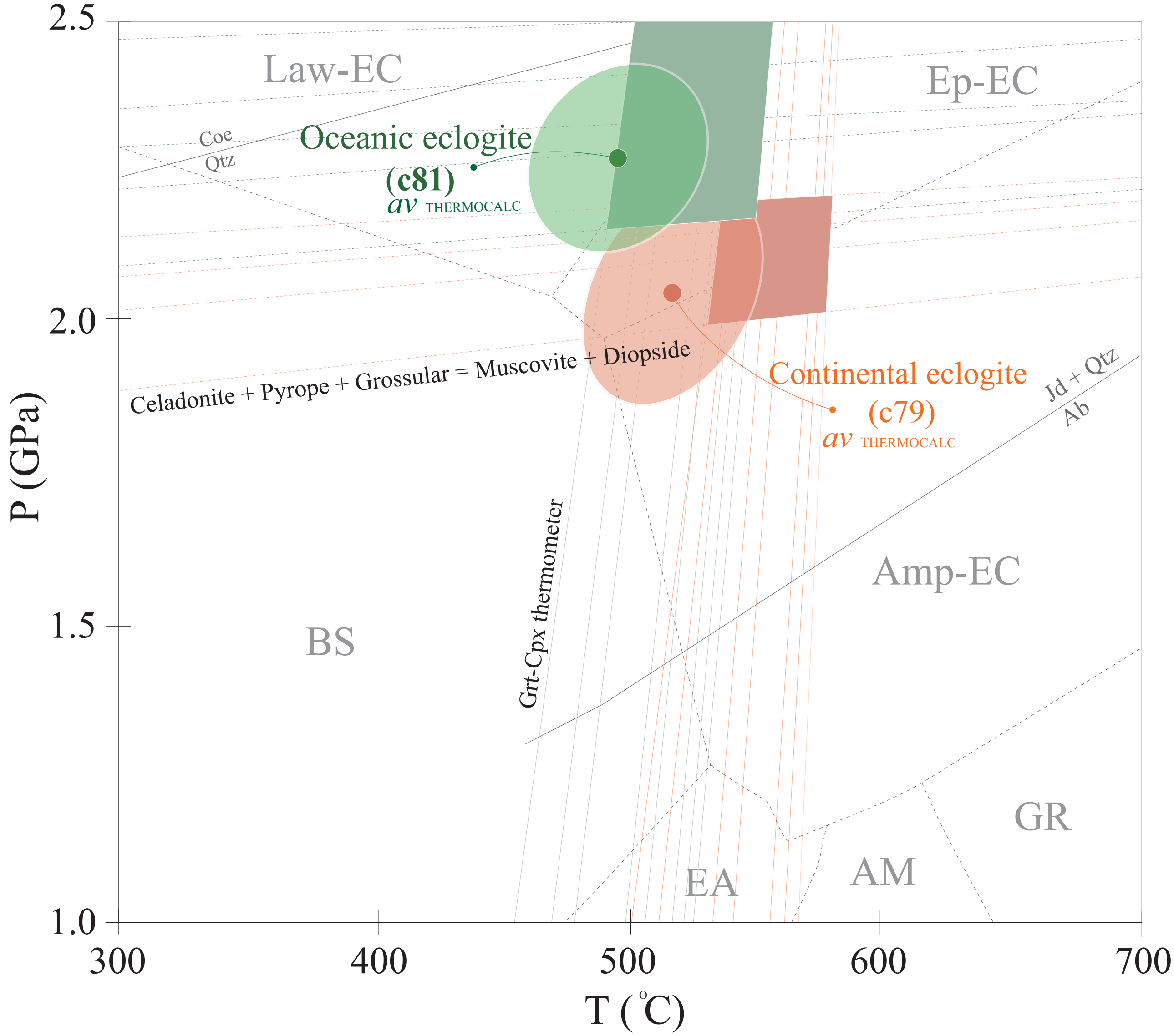

Figure 4

Cheng et al., 2014

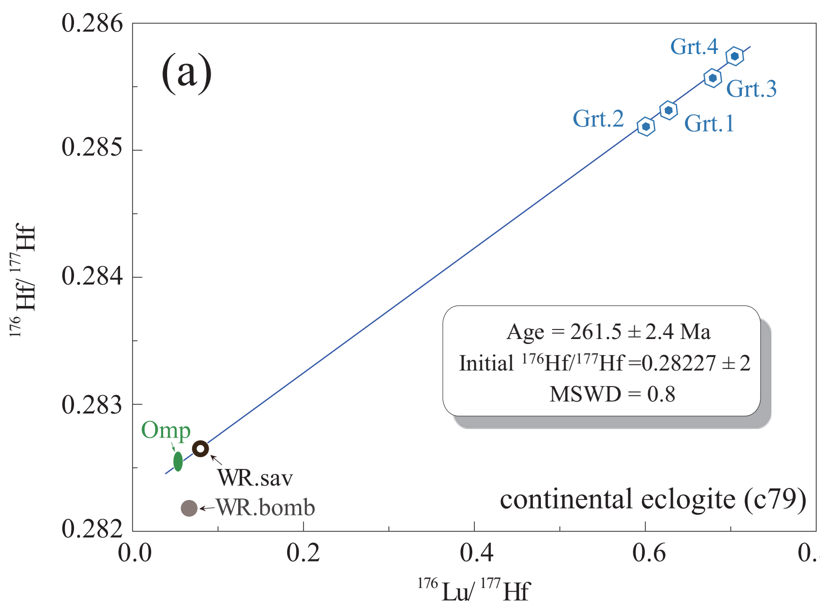

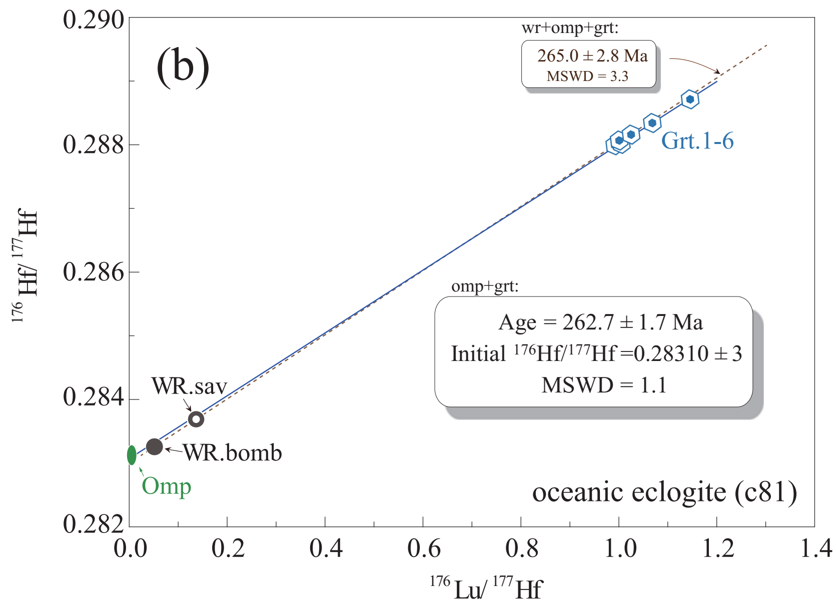

Figure 5

Cheng et al., 2014

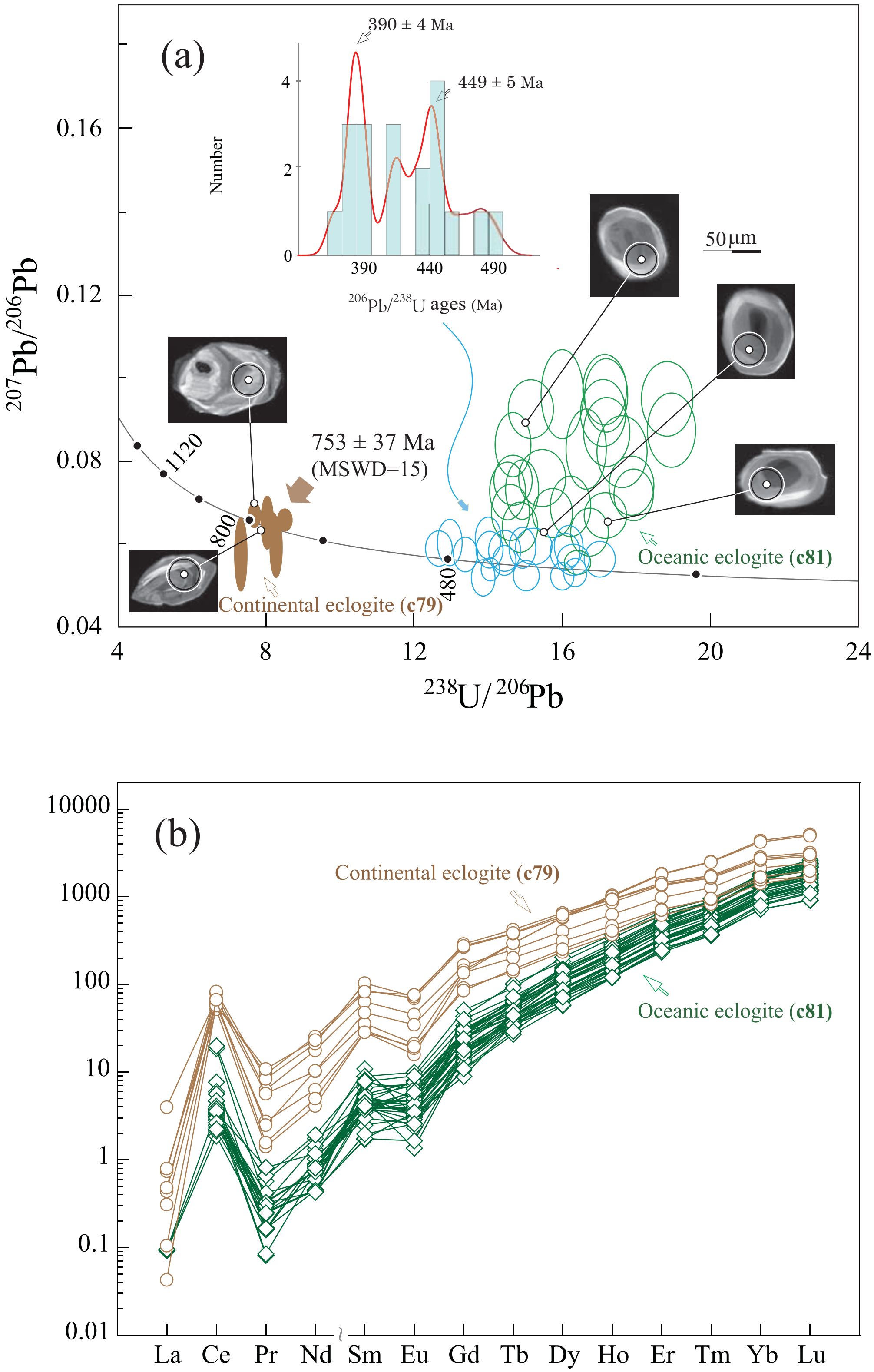

Figure 6

Cheng et al., 2014

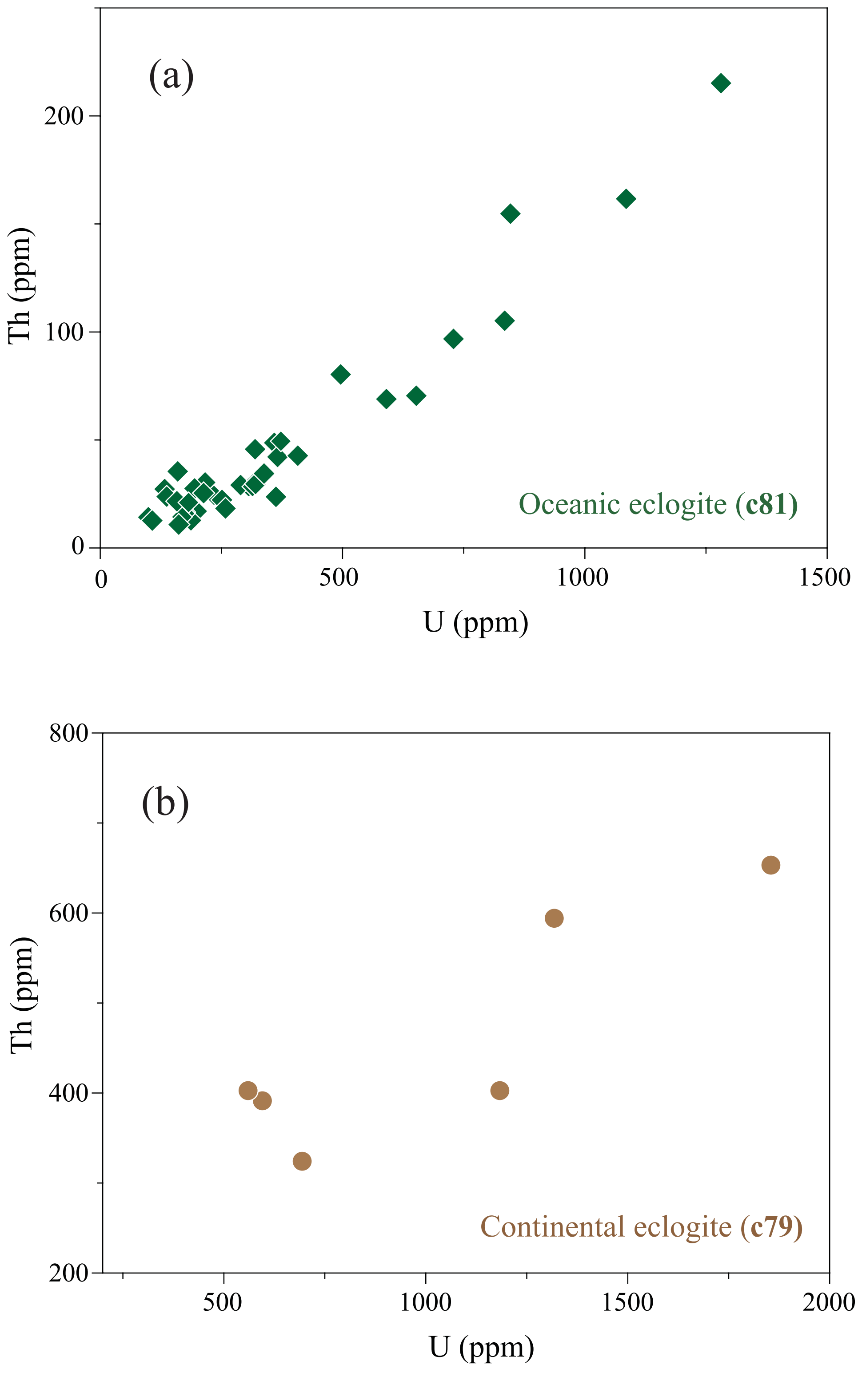

Figure 7

Cheng et al., 2014

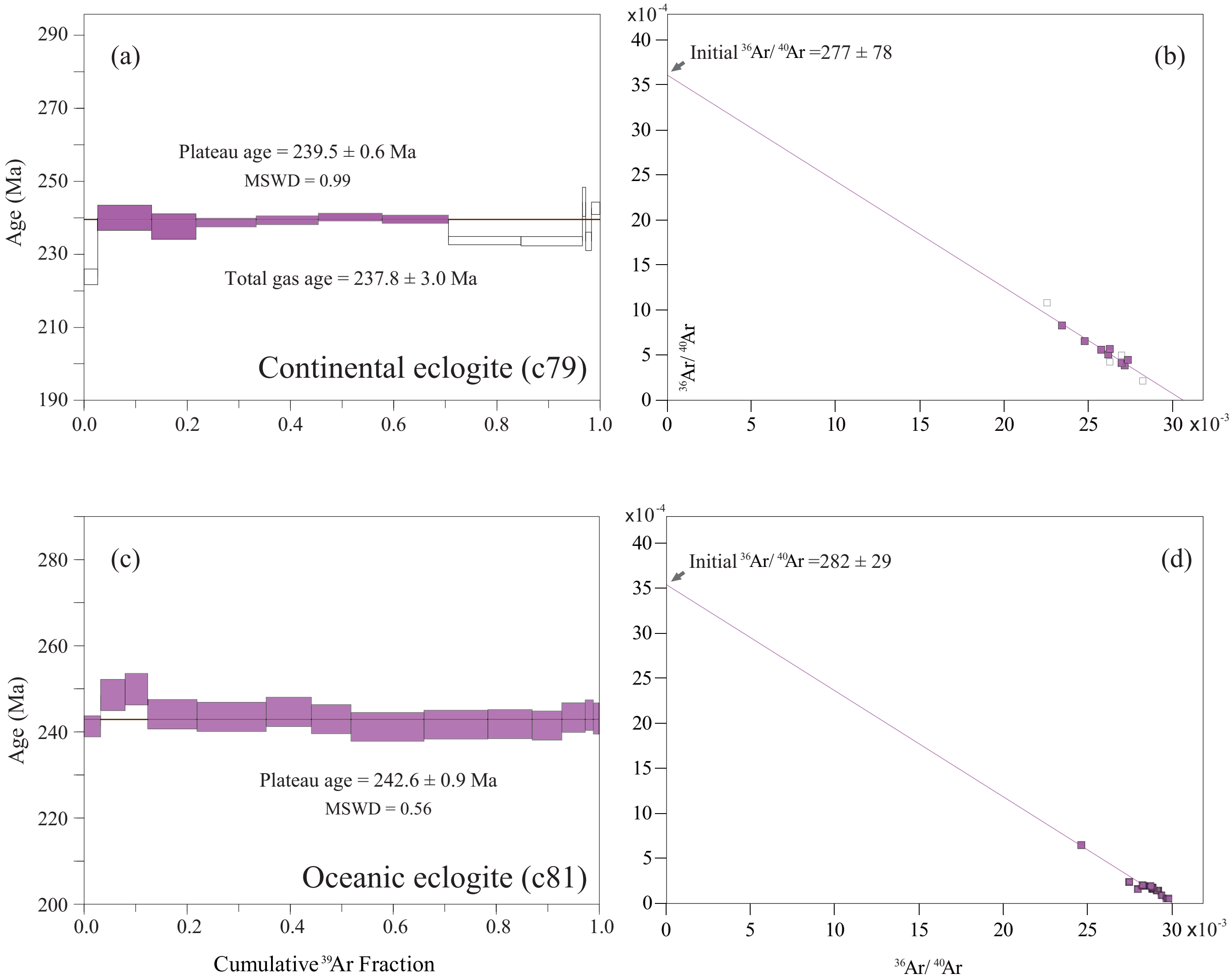

Figure 8

Cheng et al., 2014

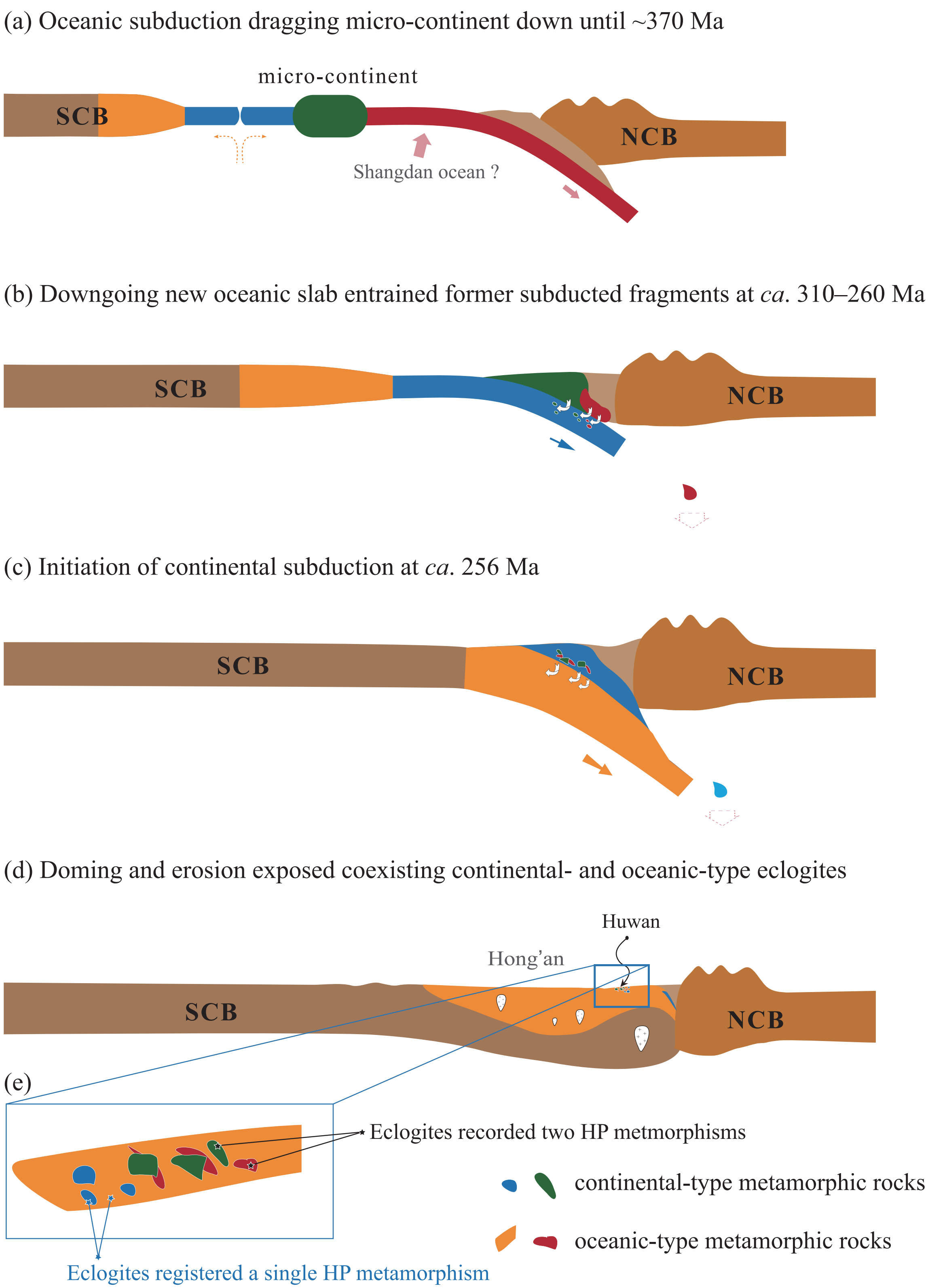

Figure 9

Cheng et al., 2014

Table 1 Chemical compositions of the Xuehe eclogite.

Sample	c79	c81
(Major oxides in wt.%)		
SiO_2	48.09	46.30
TiO_2	3.64	1.19
Al_2O_3	12.72	17.19
FeO^*	16.38	17.06
MnO	0.33	0.16
MgO	4.84	4.49
CaO	10.91	10.87
Na_2O	1.39	1.91
K_2O	0.13	0.31
P_2O_5	0.53	0.10
L.O.I.†	0.63	0.68
Total	98.97	99.58
(Trace elements in ppm)		
La	19.3	1.47
Ce	45.3	3.87
Pr	6.48	0.63
Nd	29.7	3.50
Sm	8.26	1.36
Eu	2.76	0.61
Gd	9.61	2.20
Tb	1.70	0.44
Dy	10.7	2.98
Ho	2.23	0.62
Er	6.23	1.74
Tm	0.89	0.25
Yb	5.55	1.59
Lu	0.86	0.24
Ba	261	67.7
Th	1.45	0.15
Nb	8.47	0.92
Y	56.7	15.7
Hf	4.61	0.60
Ta	0.53	0.05
U	0.39	0.15
Pb	6.84	8.43
Rb	19.84	8.44
Cs	0.52	0.72
Sr	228	239
Sc	42.3	52.9
Zr	187	16.6
Ni	40.3	90.9
V	405	473
Cr	17.3	423
$^{147}Sm/^{144}Nd$	0.1495	0.2315
$^{143}Nd/^{144}Nd$	0.512135	0.513015

*: Total Fe. †: Loss on ignition.

Table 2 Representative major-element data of the garnets, omphacites, phengites, epidotes and amphiboles*

Wt. %

	c79 (continental eclogite)							*c81 (oceanic eclogite)*					
Oxides	Grt c	Grt r	Omp	Phen	Ep	Amp	Oxides	Grt c	Grt r	Omp	Phen	Ep	Amp
SiO_2	37.80	38.39	54.65	54.28	39.46	50.92	SiO2	37.00	37.34	54.37	54.54	39.04	46.37
TiO_2	0.19	0.06	0.05	0.26	0.26	0.14	TiO2	0.02	0.01	0.04	0.26	0.11	0.15
Al_2O_3	20.06	20.78	8.52	26.54	26.99	8.96	Al2O3	21.16	21.49	7.34	25.44	25.01	11.84
FeO	22.47	28.32	5.56	1.95	6.62	13.56	FeO	24.72	27.88	7.73	2.26	8.43	15.69
MnO	7.66	0.28	–	–	–	0.04	MnO	3.44	0.16	–	–	–	0.05
MgO	0.76	4.49	8.77	4.05	0.20	12.39	MgO	0.88	2.33	8.45	4.35	0.08	10.18
CaO	10.54	7.03	14.62	–	22.26	7.04	CaO	12.24	10.40	15.02	–	22.55	8.14
Na_2O	–	–	5.73	0.53	0.05	4.26	Na2O	–	–	5.52	0.48	–	4.66
K_2O	–	–	–	9.28	–	0.18	K2O	–	–	–	9.21	–	0.25
Total	99.49	99.36	99.99	96.89	95.85	97.50	Total	99.46	99.61	99.79	96.55	95.24	97.32
Ions in Formula†							Ions in Formula†						
Element							Element						
Si	3.04	3.04	2.00	9.58	3.15	7.24	Si	2.97	2.97	2.00	9.67	3.17	6.79
Al	1.90	1.94	0.37	5.52	2.54	1.50	Al	2.00	2.02	0.32	5.32	2.40	2.04
Ti	0.01	0.00	0.00	0.03	0.02	0.02	Ti	0.00	0.00	0.00	0.03	0.01	0.02
Fe^{2+}	1.51	1.87	0.03	0.29	–	0.63	Fe^{2+}	1.66	1.86	0.08	0.34	–	0.42
Fe^{3+}	–	–	0.14	–	0.44	0.98	Fe^{3+}	–	–	0.16	–	0.57	1.50
Mn	0.52	0.02	–	–	–	0.01	Mn	0.23	0.01	–	–	–	0.01
Mg	0.09	0.53	0.48	1.07	0.02	2.63	Mg	0.11	0.28	0.46	1.15	0.01	2.22
Ca	0.91	0.60	0.57	–	1.90	1.07	Ca	1.05	0.89	0.59	–	1.96	1.28
Na	–	–	0.41	0.18	0.01	1.18	Na	–	–	0.39	0.16	–	1.32
K	–	–	–	2.09	–	0.03	K	–	–	–	2.08	–	0.05
Total	7.99	7.99	4.00	18.76	8.07	15.28	Total	8.03	8.02	4.00	18.76	8.12	15.64

* Representative analyses were chosen for garnet core (Grt c) and rim (Grt r). omphacite (Omp), phengite (Phen), epidote (Ep) and amphibole (Amp) numbers were produced from averaging multiple analyses.

† Stoichiometric ratios of elements based on 12 oxygen for garnet, 6 for omphacite, 30 for phengite, 12.5 for epidote, 23 for amphibole.

Table 3 Garnet REE data obtained by LA-ICPMS for the Xuehe eclogite.

(ppm)

dis.* (μm)	Pr	Nd	Sm	Eu	Gd	Tb	Dy	Ho	Er	Tm	Yb	Lu
c79												
49	bd	bd	0.02	0.02	0.30	0.22	5.30	2.18	7.86	1.26	8.73	1.21
87	bd	0.04	bd	0.05	0.46	0.31	5.89	2.01	7.66	1.08	6.88	1.10
114	0.02	0.10	0.20	0.48	2.60	0.48	7.25	2.57	8.76	1.36	9.26	1.32
147	0.05	0.11	0.05	0.04	0.60	0.38	6.14	2.26	7.81	1.30	7.92	1.11
180	0.04	0.02	0.55	1.60	6.45	1.10	9.90	2.62	9.39	1.51	9.94	1.56
213	0.07	0.04	0.75	0.27	1.16	0.32	4.97	2.56	13.2	2.53	20.8	3.60
240	0.04	0.02	0.47	1.00	4.33	0.74	6.00	2.37	12.3	2.78	27.4	5.20
273	bd	bd	0.02	0.01	0.21	0.17	3.82	2.23	13.9	2.85	23.7	4.05
289	bd	bd	bd	0.02	0.24	0.17	3.74	2.01	11.4	2.21	18.1	3.26
322	bd	bd	bd	0.04	0.17	0.16	3.77	1.68	9.05	1.63	13.0	1.89
376	0.02	0.10	0.22	0.10	0.66	0.24	3.50	1.47	7.13	1.13	8.26	1.13
403	0.08	0.04	0.08	0.05	0.37	0.18	3.79	1.58	6.48	0.96	7.53	0.97
436	0.05	0.03	bd	0.03	0.54	0.30	5.46	2.10	8.39	1.30	8.38	1.23
474	0.01	0.12	0.06	0.03	0.49	0.36	5.89	2.10	7.65	1.06	7.38	0.96
512	0.04	0.15	0.18	0.08	0.67	0.36	6.62	2.56	9.63	1.50	10.9	1.49
534	bd	bd	0.03	0.01	0.29	0.23	4.42	2.03	7.74	1.46	9.31	1.47
c81												
35	0.01	0.07	bd	0.08	0.26	0.15	4.97	1.93	8.95	1.54	12.7	1.70
52	bd	0.04	0.28	0.48	0.41	0.31	3.37	2.75	15.07	1.63	10.8	1.35
84	bd	0.14	0.11	0.06	0.63	0.47	7.79	3.02	9.43	1.40	9.56	1.05
111	0.44	2.12	0.92	0.36	1.36	0.30	5.09	2.37	11.9	2.22	17.7	2.51
136	0.00	0.01	0.01	0.01	0.15	0.14	3.04	1.78	10.7	2.13	18.5	2.95
164	0.06	0.63	0.16	0.10	0.45	0.11	3.22	2.07	15.0	4.33	49.5	9.32
191	bd	bd	bd	0.01	0.16	0.14	3.02	1.84	14.0	4.60	62.4	14.6
209	0.81	3.63	0.90	0.37	1.33	0.41	5.25	1.93	11.4	3.24	28.2	5.27
233	0.18	0.56	0.28	0.32	1.03	0.72	8.52	2.78	9.15	1.48	9.56	1.27
264	bd	bd	0.03	0.02	0.24	0.17	3.39	1.77	8.09	1.31	9.72	1.35
289	bd	bd	0.06	bd	0.41	0.17	4.00	1.86	7.49	1.15	8.44	0.87
317	0.01	0.09	0.00	0.05	0.19	0.24	3.92	1.98	7.95	1.21	9.11	1.50
341	bd	0.04	0.03	0.02	0.29	0.15	4.44	1.99	7.70	1.29	8.91	1.06

*: rim-core-rim. bd: below detection.

Table 4 Lu–Hf isotope data for the Xuehe eclogite.

Sample[a]	Lu (ppm)[b]	Hf (ppm)[b]	$^{176}Lu/^{177}Hf$ [c]	$^{176}Hf/^{177}Hf$ [d]
c79 (continental eclogite)				
Grt.1	0.726	0.171	0.601	0.285200 ± 6
Grt.2	0.694	0.172	0.572	0.285072 ± 5
Grt.3	0.759	0.153	0.705	0.285740 ± 5
Grt.4	1.00	0.204	0.680	0.285582 ± 6
Omp	0.0494	0.113	0.0565	0.282553 ± 5
WR.bomb	0.303	4.61	0.0622	0.282257 ± 3
WR.sav	0.415	1.04	0.0795	0.282650 ± 4
c81 (oceanic eclogite)				
Grt.1	0.523	0.0741	1.00	0.288020 ± 6
Grt.2	0.500	0.0709	1.00	0.288066 ± 8
Grt.3	0.521	0.0692	1.07	0.288341 ± 6
Grt.4	0.755	0.0689	1.15	0.288722 ± 7
Grt.5	0.531	0.0755	1.00	0.288007 ± 5
Grt.6	0.503	0.0697	1.03	0.288158 ± 6
Omp	0.0206	0.462	0.00635	0.283132 ± 5
WR.bomb	0.225	0.540	0.0591	0.283335 ± 3
WR.sav	0.308	0.320	0.136	0.283694 ± 4

[a] Grt, garnet fraction; Omp, omphacite fraction;WR.bomb, whole rock bomb dissolution; WR.sav, whole-rock savillex dissolution.

[b] Lu and Hf concentrations determined by isotope dilution with uncertainties estimated to be better than 0.5%.

[c] Uncertainties for $^{176}Lu/^{177}Hf$ for the purpose of regressions and calculations is estimated to be 0.5%.

[d] $^{176}Hf/^{177}Hf$ ratios were corrected for instrumental mass bias using $^{179}Hf/^{177}Hf$ =0.7935 and normalized relative to $^{179}Hf/^{177}Hf$ = 0.282160 for JMC-475. Reported errors on the $^{176}Hf/^{177}Hf$ are within-run 2σ, standard error, and are given in the 6th decimal place. Errors calculated for ages (not shown) are based on external reproducibility of spiked wholerock samples ($^{176}Hf/^{177}Hf$ =0.01%) and within run errors (as reported above) added in quadrature.